RESEARCH ARTICLE

Key Points:
- Strong Agulhas Leakage during Termination II affected upper ocean salinity of the western South Atlantic
- The tropical ocean-atmosphere configuration induced recirculation of Agulhas waters within the South Atlantic subtropical gyre
- Two intervals of strong freshening of the upper Brazil Current suggests northward transmission of dense waters during the Last Interglacial

Supporting Information:
- Supporting Information S1

Correspondence to:
A. L. S. Albuquerque,
ana_albuquerque@id.uff.br

Tracking Spread of the Agulhas Leakage Into the Western South Atlantic and Its Northward Transmission During the Last Interglacial

João M. Ballalai[1] [ID], Thiago P. Santos[1] [ID], Douglas O. Lessa[1] [ID], Igor M. Venancio[2] [ID], Cristiano M. Chiessi[3] [ID], Heather J. H. Johnstone[4] [ID], Henning Kuhnert[4] [ID], Marcela R. Claudio[1] [ID], Felipe Toledo[5] [ID], Karen B. Costa[5] [ID], and Ana Luiza S. Albuquerque[1] [ID]

[1]Programa de Geociências (Geoquímica), Universidade Federal Fluminense, Niterói, Brazil, [2]Center for Weather Forecasting and Climate Studies (CPTEC), National Institute for Space Research (INPE), Cachoeira Paulista, Brazil, [3]Escola de Artes, Ciências e Humanidades, Universidade de São Paulo, São Paulo, Brazil, [4]MARUM-Center for Marine Environmental Sciences, University of Bremen, Bremen, Germany, [5]Laboratório de Paleoceanografia do Atlântico Sul, Instituto Oceanográfico, Universidade de São Paulo, Brazil

Abstract Intensification of the Agulhas Leakage (AL) during glacial terminations has long been proposed as a necessary mechanism for reverting the Atlantic Meridional Overturning Circulation (AMOC) to its interglacial mode. However, lack of records showing the downstream evolution of AL signal and substantial temporal differences between AL intensification and resumption of deep-water convection have cast doubt on the importance of this mechanism to the AMOC. Here, we analyze a combination of new and previously published data relating to Mg/Ca-derived temperatures and ice volume-corrected seawater $\delta^{18}O$ records ($\delta^{18}O_{IVC-SW}$, as a proxy for relative changes in ocean salinity), which demonstrate propagation of AL signal via surface and thermocline waters to the western South Atlantic (Santos Basin) during Termination II and the early Last Interglacial. The saline AL waters were temporally stored in the upper subtropical South Atlantic until they were abruptly released in two stages into the North Atlantic via surface and thermocline waters at ca. 129 and 123 ka BP, respectively. Accounting for age model uncertainties, these two stages are coeval with the resumption of convection in the Labrador and Nordic seas during the Last Interglacial. We propose a mechanism whereby both active AL and a favorable ocean-atmosphere configuration in the tropical Atlantic were required to allow flux of AL waters into the North Atlantic, where they then contributed to enhancing the AMOC during the Last Interglacial period. Our results provide a framework that connects AL strengthening to the AMOC intensifications that followed glaciations.

Plain Language Summary During the Quaternary period, the Earth's climate fluctuated between glacial and interglacial states. Such climate transitions, known as glacial terminations, were characterized by rapid changes in ice-volume, atmospheric CO_2 levels, and global temperatures. Several geochemical and modeling studies have demonstrated that the Atlantic Meridional Overturning Circulation (AMOC) was strongly inhibited during these periods. In general, meltwater discharge due to ice-sheet retraction at high latitudes of the North Atlantic seems to have weakened deep-ocean convection and affected northward transport of heat and salt. To return the AMOC to a fully active mode, the impact of that meltwater had to be counterbalanced. Previous investigations suggested that leakage of salty waters from the Indian Ocean into the South Atlantic (Agulhas Leakage, AL) during glacial terminations played a prominent role in reinstating northward heat and salt transport. However, it is not clear how far into the South Atlantic the influence of the AL can be tracked and how, in terms of timing, it is linked to resumption of deep-water convection. Here, we focus on glacial Termination II to demonstrate AL signal in the western South Atlantic and how it contributed to enhancing the AMOC during the Last Interglacial.

1. Introduction

The Atlantic Meridional Overturning Circulation (AMOC) is a crucial feature of the global climate system, which plays a critical role in inter-hemispheric connectivity through northward upper-ocean transport of warm and saline waters (Cunningham et al., 2007). In the high latitudes of the North Atlantic, these

waters lose heat to the atmosphere, sink, and then flow southward, carrying cold saline waters into the Southern Ocean (Kuhlbrodt et al., 2007). This exchange is a central component of the meridional circulation and it takes place via the Agulhas Leakage (AL) (Gordon, 1985). The saline waters of the AL are a significant contributor to the negative buoyancy of the AMOC and they are carried towards the subpolar North Atlantic by means of the upper limb of the meridional circulation, thereby maintaining the salinity, strength, and stability of deep-water convection (Biastoch et al., 2008; Weijer et al., 2001).

The AL principally enters the South Atlantic as thermocline waters through spreading of rings and filaments incorporated into the South Atlantic Central Water (SACW) (de Ruijter et al., 1999; Donners & Drijfhout, 2004). This water mass fills most of the South Atlantic between depths of 100 and 600 m (Peterson & Stramma, 1991). Once in the South Atlantic, convection and air-sea interactions modify AL signal, with advection westwards strengthening its positive salt anomaly (Weijer, 2002). This process results in the South Atlantic thermocline being saltier in areas influenced by the AL (Byrne et al., 1995). The AL signal may propagate into the Northern Hemisphere via Kelvin waves generated along the western boundary of the Atlantic Ocean, so regions of the Brazilian margin may accurately record the timing of changes in overturning circulation associated with changes in the AL (van Sebille & van Leeuwen, 2007; Weijer et al., 2002). Thus, both the Brazil Current (BC) and North Brazil Current (NBC) play essential roles in inter-hemispheric transmission of AL signal. Since partitioning of salt and heat between the BC and NBC depends on the position of the South Equatorial Current (SEC) bifurcation (Marcello et al., 2018), the latitudinal position of that bifurcation can be considered a type of ocean gateway. That gateway controls how much subtropical water (partially comprising eastern South Atlantic AL waters) flows northward across the equator via the NBC and how much is recirculated into the subtropical gyre via the BC (Marcello et al., 2018).

Paleoceanographic reconstructions suggest that the AL was reduced during glacial stages because of the northerly position of the South Atlantic's oceanic Subtropical Front and expansion of Antarctic sea ice (Bard & Rickaby, 2009; Peeters et al., 2004). Near the end of extended glacial periods, the position of the Subtropical Front shifted southward increasing AL volume (Caley et al., 2014; Cortese et al., 2007; Peeters et al., 2004). Intensification of the AL preceding glacial terminations suggests that salt and heat oscillations across the Indian-South Atlantic exchange, combined with effective northward transmission of these waters, could have fundamentally influenced the buoyancy of the upper North Atlantic waters after glacial maxima and, consequently, such oscillations may have played a critical role in the AMOC reverting to its interglacial mode (Beal et al., 2011; Caley et al., 2012). However, scarcity of marine records capturing downstream progression of AL signal, as well as the considerable time difference between AL strengthening and AMOC resumption, have prevented broad acceptance of this mechanism. For example, during the transition from the penultimate glacial (i.e., Marine Isotope Stage, MIS 6) to the Last Interglacial (MIS 5e), records from the eastern South Atlantic on Mg/Ca-derived sea surface temperature (SST) and ice-volume-corrected seawater $\delta^{18}O$ ($\delta^{18}O_{IVC-SW}$, as a proxy for relative changes in ocean salinity) suggest the AL intensified from as early as ca. 142 ka BP (Scussolini et al., 2015). However, some deep-water convection in high latitudes of the North Atlantic apparently did not strengthen until late into glacial Termination II (TII), ca. 129 ka BP (Deaney et al., 2017). This interval of approximately 13 kyr suggests that AL waters were not directly transported into regions of deep-water formation, so other ocean gateways must have played fundamental roles in connecting the AL to the North Atlantic.

Here, we present new thermocline Mg/Ca-derived temperature and $\delta^{18}O_{IVC-SW}$ data from the western South Atlantic for the transition between MIS 6 and MIS 5e based on planktic *Globorotalia inflata* foraminifera. We then combine our new data with published surface $\delta^{18}O_{IVC-SW}$ data from the same core (Santos et al., 2017b). Comparison of these new (thermocline) and published (surface) data with data from previous studies on the eastern South Atlantic suggests that AL waters accumulated in the South Atlantic subtropical gyre and were released into the North Atlantic in two stages during the Last Interglacial. We propose a mechanism whereby the saline waters injected by the AL were retained in the upper subtropical South Atlantic throughout TII and then released into the Northern Hemisphere in two pulses during the early- and mid-Last Interglacial. These pulses induced rapid reductions in salinity of the western South Atlantic that were coeval to periods of resumed deep-water formation. Thus, our results link the AL to sites of North Atlantic Deep Water (NADW) formation.
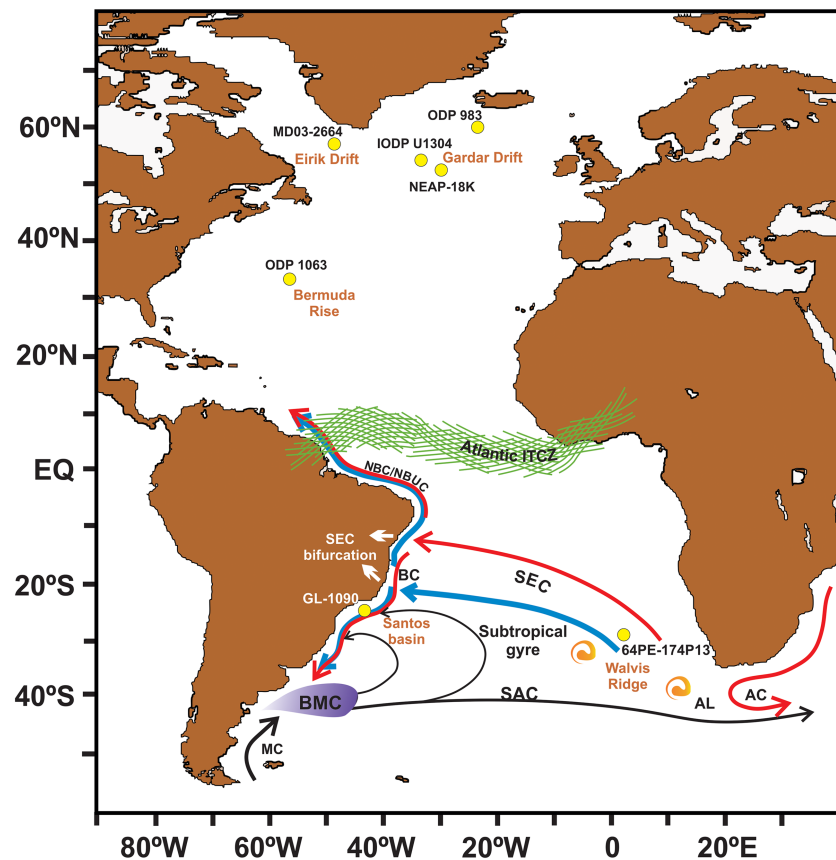
Figure 1. - Schematic representation of mean circulation of the South Atlantic subtropical gyre (based on Stramma & England, 1999), the Agulhas Current (AC), and the mean position of the Intertropical Convergence Zone (ITCZ). The most relevant surface and thermocline currents for this study are shown by thick red and blue lines, respectively. The South Equatorial Current (SEC) exhibits a southward shift at thermocline levels (represented by the thick blue line), as described in Stramma and England (1999) and Rodrigues et al. (2007). Note that bifurcation of the SEC at the thermocline occurs at a higher latitude relative to the surface bifurcation. NBC/NBUC: North Brazil Current/Undercurrent; BC: Brazil Current; MC: Malvinas Current; BMC: Brazil-Malvinas Confluence; SAC: South Atlantic Current; AL: Agulhas Leakage. The yellow dots mark the positions of core GL-1090 (this study) and other relevant records discussed in the text: 64PE-174P13 (Scussolini et al., 2015), ODP Site 1063 and 983 (Deaney et al., 2017), ODP Site 1058 (Bahr et al., 2013), MD03-2664 (Irvalı et al., 2016), NEAP-18K (Hall et al., 1998), and IODP Site U1304 (Hodell et al., 2009).

2. Study Area

Core GL-1090 (24.92 °S, 42.51 °W, 2225 m water depth, 1914 cm long) was collected by the Petrobras oil company in the western South Atlantic (Santos Basin – Figure 1). The uppermost circulation in the area (0 – 600 m) is dominated by the BC, which is the western boundary current that closes the subtropical gyre of the South Atlantic (Peterson & Stramma, 1991) (Figure 1). The southward flow of the BC transports two water masses: (1) at the surface, where the upper layer (ca. 0 – 100 m) of the BC is composed of warm (> 20 °C) and saline (> 36) Tropical Water due to the high incoming solar radiation and excess evaporation that characterize the tropical South Atlantic (Campos et al., 1995); and (2) below the Tropical Water (ca. 100 – 600 m), where the BC transports the colder (6 – 20 °C) and less saline (> 34.6 – 36) SACW that fills the South Atlantic thermocline. Apart from their temperatures and salinities, these two water masses can also be distinguished by the $\delta^{13}C$ levels of their dissolved inorganic carbon ($\delta^{13}C_{DIC}$), with $\delta^{13}C_{DIC} = 1.74 \pm 0.24$ ‰ and $\delta^{13}C_{DIC} = 1.30 \pm 0.22$ ‰ for the Tropical Water and SACW, respectively (Venancio et al., 2014). This difference in $\delta^{13}C$ is due to the higher nutrient content of central waters, with $\delta^{13}C_{DIC}$ values decreasing with increasing nutrient concentration (Broecker & Maier-Reimer, 1992). The SACW forms in the mid-latitudes of the South Atlantic via air-sea interactions in the Brazil-Malvinas Confluence (where the southernmost extension of the BC meets the Malvinas Current) and in the areas adjacent to the Argentine basin and

mid-Atlantic ridge along the South Atlantic Current (Garzoli & Matano, 2011). The central waters of the South Atlantic are also composed of Indian Ocean Central Water brought to the South Atlantic by the AL in the upper 1000 m of the water column (Richardson, 2007).

The BC originates from the southern branch of the SEC where it bifurcates near the western slope of the Brazil Basin (Peterson & Stramma, 1991). The surface latitude of that bifurcation varies between ca. 10 – 15 °S (Lothar Stramma, 1991), and it tends to shift northward during the austral spring and summer when the Intertropical Convergence Zone (ITCZ) shifts southward and the northeasterly trade-winds are stronger (Rodrigues et al., 2007). These conditions lead to the highest intensity of the BC flux. The northwestward flow of the NBC is also generated from the SEC bifurcation (Figure 1). The NBC transports warm saline waters into the North Atlantic (Johns et al., 1998), and its transport is also marked by seasonal variability that contrasts with the conditions that enhance the BC (Silva et al., 2009). A particular feature of the NBC is that it flows as an undercurrent between 5 °S and 10 °S (the North Brazil Undercurrent) and only assumes the character of a surface flow north of 5 °S (Stramma et al., 1995). It is also essential to highlight the fact that mean circulation of the South Atlantic subtropical gyre manifests a southward shift with increasing depth, such that the SEC bifurcation occurs as far south as 20 °S at depths of 500 m (Rodrigues et al., 2007; Stramma & England, 1999).

3. Materials and Methods

3.1. New and Published Data From Core GL-1090

Core GL-1090 was first described by Santos et al., 2017b, and its 1914 cm length covers the last 185 ka BP. In this study, we report a new reconstruction of the thermocline Mg/Ca-derived temperature and $\delta^{18}O_{IVC-SW}$ profile for the Santos Basin for the period between 140 and 110 ka BP based on planktic *G. inflata* foraminifera (see section 3.2). This chronological interval lies between 1495 and 1332 cm of core GL-1090. Estimation of the thermocline $\delta^{18}O_{IVC-SW}$ profile was based on $\delta^{18}O$ values for *G. inflata* calcite, as published by Santos et al. (2017a) (see section 3.2). In addition to this new data, we also include published surface $\delta^{18}O_{IVC-SW}$ values from the same core but with a novel interpretation focused on TII and interhemispheric connections. We have also used surface $\delta^{18}O_{IVC-SW}$ data from GL-1090 based on *Globigerinoides ruber* to produce a revised age model for the interval between 1495 and 1332 cm that preserves the original sedimentation characteristics presented by Santos et al. 2017b but reduces the age uncertainty around the penultimate glacial-interglacial transition (see section 3.3).

3.2. Calculation of Thermocline Temperature and Ice-Volume-Corrected Seawater $\delta^{18}O$

Mg/Ca measurements were performed on samples comprising 9-30 individuals of planktic *G. inflata* foraminifera from the 250-300 μm size fraction. A previous plankton tow study at the central Walvis Ridge (eastern South Atlantic) suggested that the base of the calcification depth of this species lies between 300 and 400 m in summer and winter, respectively (Lončarić et al., 2006). Based on a transect of surface sediment samples at the Brazil-Malvinas Confluence (western South Atlantic), Chiessi et al. (2007) proposed that *G. inflata* $\delta^{18}O$ data are consistent with a calcification depth between 200 and 400 m. In the North Atlantic, *G. inflata* preferentially live at the base of the summer thermocline, which lies approximately 100 m north of 35 °N, whereas the species calcifies deeper (at ca. 250 m) in the warmer conditions south of 35 °N (Cléroux et al., 2007). Thus, we assume a thermocline habitat for *G. inflata* that is within the SACW in the Santos Basin. Furthermore, the distribution of *G. inflata* is relatively constant throughout core GL-1090, making it better suited to characterizing thermocline temperatures than other deep-dwelling planktic foraminiferan species (e.g., *Globorotalia truncatulinoides* or *Globorotalia crassaformis*).

The tests of *G. inflata* were gently crushed between two clean glass plates to open the chambers, and they were cleaned according to the protocol of Barker et al. (2003). These broken tests underwent ultrasonic cleaning alternated between multiple washes in deionized water and ethanol to remove clay contaminants. Hydrogen peroxide treatment in a boiling water bath was performed to eliminate organic matter, and a short treatment of dilute acid (0.001 M nitric acid) leaching was performed to eliminate any adsorbed contaminants. Next, the samples were dissolved in 0.075 M nitric acid. The dissolved samples were centrifuged for 10 min to exclude insoluble residues. The diluted solutions were analyzed at MARUM – Center for Marine Environmental Sciences (University of Bremen, Germany) with an Inductively Coupled Plasma Optical Emission

Spectrometer (ICP-OES) (Agilent Technologies 700 Series) with a Cetac ASX-520 autosampler and a micro-nebulizer. Three repeated measurements of each sample were run, and the results were averaged. Elements were measured at the following spectral lines: Mg (279.6 nm), Ca (315.9 nm), Sr (421.6), Al (167.0 nm), Fe (238.2 nm), and Mn (257.6 nm). The calibration standards consisted of dissolution acid (0.075 M HNO_3) as a blank and four multielement standards between 20 and 80 ppm Ca, with Mg/Ca of 4.12 mmol/mol. The calibrations for all elements were based on linear regressions. Instrumental precision was monitored via runs of an in-house external standard solution after approximately every five samples. The long-term relative standard deviation of the in-house standard is <2 % for the Mg/Ca ratio. A dissolved solution of the ECRM 752-1 commercial limestone standard was also measured twice. This solution was measured at 3.73 mmol/mol ($\sigma = 0.01$, 0.24%) during the ICP-OES run, which is very close to the published value of 3.75 for a centrifuged solution (Greaves et al., 2005). We analyzed 64 Mg/Ca samples from the time interval between 140–110 ka BP.

Three samples had values of Ca <10 ppm, so these were rejected since the calibration is non-linear at low Ca concentrations. The Al/Ca, Fe/Ca, and Mn/Ca ratios of the remaining samples were analyzed to monitor cleaning efficiency (Supplementary Table S1). These samples showed average Al/Ca, Fe/Ca, and Mn/Ca ratios of 0.26, 0.19, and 0.29 mmol/mol, respectively. This mean Al/Ca ratio is below the commonly accepted limits of 0.3–0.5 mmol/mol (Kuhnert et al., 2014; Lea et al., 2005). The mean Fe/Ca and Mn/Ca ratios are slightly higher than the 0.1 mmol/mol threshold proposed by Barker et al. (2003). However, the weak correlation of our Mg/Ca ratio to both the Fe/Ca ($R^2 = 0.09$) and Mn/Ca ($R^2 = 0.04$) ratios (Figure S1) suggests that our analyses are not likely to have been significantly affected by Fe–Mn oxyhydroxides. Other studies have also reported values for Fe/Ca and Mn/Ca ratios higher than those given by Barker et al. (2003) (e.g., Groeneveld et al., 2008; Steinke et al., 2010; Vázquez Riveros et al., 2016; Weldeab et al., 2006). These studies consider that the input of terrigenous material rich in Fe–Mn oxyhydroxides relative to biogenic carbonates affects Fe/Ca and Mn/Ca ratios. This scenario may also apply in the western South Atlantic, which receives contributions of highly weathered soils enriched in Fe–Mn oxyhydroxides from continental South America (Govin, Holzwarth, et al., 2012). Furthermore, the cleaning protocol of Barker et al. (2003) is considered to be less efficient at removing Fe–Mn oxyhydroxides compared to those incorporating an additional reductive step (e.g., Martin & Lea, 2002). Steinke et al. (2010) tested both of these protocols on samples with much higher Fe/Ca and Mn/Ca values than ours (up to 0.96 and 1.65 mmol/mol of Fe/Ca and Mn/Ca, respectively) and found no apparent difference in terms of Mg/Ca ratios. Accordingly, we assume that our temperature reconstruction is not affected by contaminating clays.

Several calibrations are available to convert *G. inflata* Mg/Ca ratios into temperature (e.g., Anand et al., 2003; Cléroux et al., 2008, 2013; Elderfield & Ganssen, 2000; Groeneveld & Chiessi, 2011; McKenna & Prell, 2004; Regenberg et al., 2009). Species-specific and regionally constrained equations provide more accurate estimates of Mg/Ca paleotemperature (Anand et al., 2003). Thus, the studies of Groeneveld and Chiessi (2011) and Cléroux et al. (2013) offer appropriate equations for our study since they included South Atlantic core-top samples in their species-specific calibrations for *G. inflata*. However, some factors hamper use of both these latter calibrations. Groeneveld and Chiessi (2011) discriminated between encrusted and non-encrusted specimens. Differentiation of such samples from core GL-1090 would result in an insufficient number of *G. inflata* shells to perform Mg/Ca analyses. Offsets of up to 7 °C between the different encrustation states were reported by Groeneveld and Chiessi (2011), so adopting their calibration approach could introduce significant bias into our analysis. Cléroux et al. (2013) did not discriminate between encrusted and non-encrusted *G. inflata* shells, but nor did they apply the cleaning protocol of Barker et al. (2003). Cléroux et al. (2013) suggested that their different cleaning procedure likely explained the lower pre-exponential constant obtained in their analysis compared to those of other calibrations. Consequently, the calibration of Cléroux et al. (2013) resulted in temperatures that we judge to be unrealistically cold for the Santos Basin thermocline. For these reasons, we chose the calibration of Cléroux et al. (2008) given by [Mg/Ca = 0.71 exp 0.06*(T)]. This equation was developed using North Atlantic core-tops and was calibrated within an isotopic temperature range (10.5–17.9 °C) similar to that found in the Santos Basin thermocline. Cléroux et al. (2008) also applied the cleaning protocol of Barker et al. (2003), which generated a pre-exponential constant more consistent with those obtained via other calibration studies. Moreover, some of the elemental trace measurements were made on size fractions of 250–315 μm (Cléroux et al., 2008). That size fraction is similar to the one we selected in this study, consequently reducing the potential error associated with a size effect (Cléroux et al., 2008).
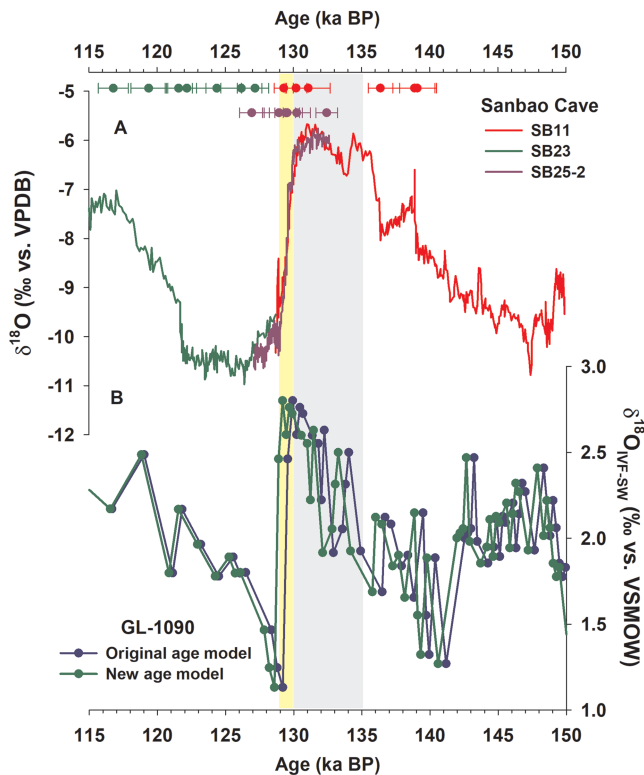
Figure 2. - Alignment between the Santos Basin surface $\delta^{18}O_{IVF-SW}$ values with records of the Asian Monsoon from Sanbao Cave, together with their respective radiometrically-determined [230]Th ages (Wang et al., 2008). The revised age model of core GL-1090 (green) generates slightly younger ages across the transition to the Last Interglacial compared with the prior age-model for this section (blue, Santos et al., 2017b). The grey bar highlights the period of weak Asian Monsoon that corresponds to Heinrich Stadial 11, and the yellow bar highlights the transition to a strong Asian Monsoon at the onset of the Last Interglacial.

We applied the temperature-$\delta^{18}O$ relationship given by the equation [T = 16.9 − 4.0 ($\delta^{18}O_C$ − $\delta^{18}O_{SW}$)] (Shackleton, 1974) to estimate the seawater $\delta^{18}O$ composition ($\delta^{18}O_{SW}$) of the thermocline. We also used the calcite $\delta^{18}O$ of *G. inflata* for the transition between MIS 6 and MIS 5e published by Santos et al. (2017a) for core GL-1090. A conversion factor of 0.27 ‰ was applied to convert values from the VPDB standard to Vienna Standard Mean Ocean Water (VSMOW). The effect of changes in global sea level was subtracted from the $\delta^{18}O_{SW}$ values by applying the sea level correction of Grant et al. (2012). This operation yielded an ice-volume-corrected seawater oxygen isotopic composition ($\delta^{18}O_{IVC-SW}$) that we used as a proxy for relative changes in thermocline salinity. The $\delta^{18}O_{IVC-SW}$ error estimation combines an uncertainty of 1.4 °C for the *G. inflata* Mg/Ca calibration (Cléroux et al., 2008) (which is equivalent to a 0.30 ‰ $\delta^{18}O$ change) plus an analytical error for *G. inflata* $\delta^{18}O$ of 0.06 ‰ (Santos et al., 2017a). Thus, the propagated cumulative root-mean-square error estimated for the $\delta^{18}O_{IVC-SW}$ is 0.31 ‰, consistent with those of other studies (e.g., Gebregiorgis et al., 2016).

3.3. Age Model

The Bayesian age model (Blaauw & Christen, 2013) of core GL-1090 was obtained through a combination of calibrated AMS ^{14}C ages and benthic foraminifera $\delta^{18}O$ tie-points aligned to two reference curves (Govin et al., 2014; Lisiecki & Raymo, 2005). Most of the benthic $\delta^{18}O$ tie-points were obtained by aligning GL-1090 with core MD95-2042, which has been updated to the AICC2012 ice core chronology (Bazin et al., 2013; Govin et al., 2014; Veres et al., 2013). This chronology is the most appropriate age reference for displaying marine and ice core records over the Last Interglacial because of its numerous new stratigraphic links that significantly reduce dating uncertainty (Capron et al., 2014; Govin et al., 2015). In the original version of the GL-1090 age model (Santos et al., 2017b), an abrupt 1.67 ‰ decrease in surface $\delta^{18}O_{IVC-SW}$ at the end of TII occurred immediately after 129.9 ka BP (1404 cm), with a mean estimated age uncertainty of ± 3.87 ka. Assuming that the salinity mechanism discussed here is correct, i.e., that the coupling between the ITCZ and SEC bifurcation controls surface (subtropical gyre) and thermocline (subtropical cell) salinity in the western South Atlantic, we used one of the [230]Th ages from Sanbao Cave (SB11) (Wang et al., 2008) as a tie-point for the transition at the end of TII. Wet and dry conditions in Sanbao Cave have also been associated with the north-south migration of the tropical rain belt represented by the ITCZ (Wang et al., 2008). In Sanbao Cave, $\delta^{18}O$ values indicate a shift from arid conditions at 129.6 ka BP (ca. -6.9‰) to a wet climate at 128.8 ka BP (ca. -10‰). The nearest [230]Th age is located at 129.3 ± 0.7 ka BP (ca. -8‰), which is approximately midway between weak and strong monsoons. Next, we removed a previous tie-point located at 1403 cm (Santos et al., 2017b) and aligned the [230]Th age of 129.3 ± 0.7 ka at 1402 cm (midway along the surface $\delta^{18}O_{IVC-SW}$ transition) as a new tie-point for core GL-1090 (Figure 2). This exercise did not alter the previously estimated accumulation rate or produce significantly different ages for other parts of core GL-1090 (Figure S2).

This minor modification slightly delayed to 129.1 ka BP the onset of the surface $\delta^{18}O_{IVC-SW}$ transition at 1404 cm (Figure 2), considerably reducing mean uncertainty from ± 3.87 ka (original age model, Santos et al., 2017b) to ± 1.51 ka (Figure S3). Our new data relating to the Santos Basin reveal that the thermocline $\delta^{18}O_{IVC-SW}$ declined later than that at the surface, i.e., at 122.9 ka BP (1375 cm – see section 4). The mean Bacon uncertainty estimated for around this depth was ± 4.8 ka based on the prior age model (Figure S3). Through our reevaluation, the age uncertainty around this depth has been slightly reduced to ± 4.35 ka
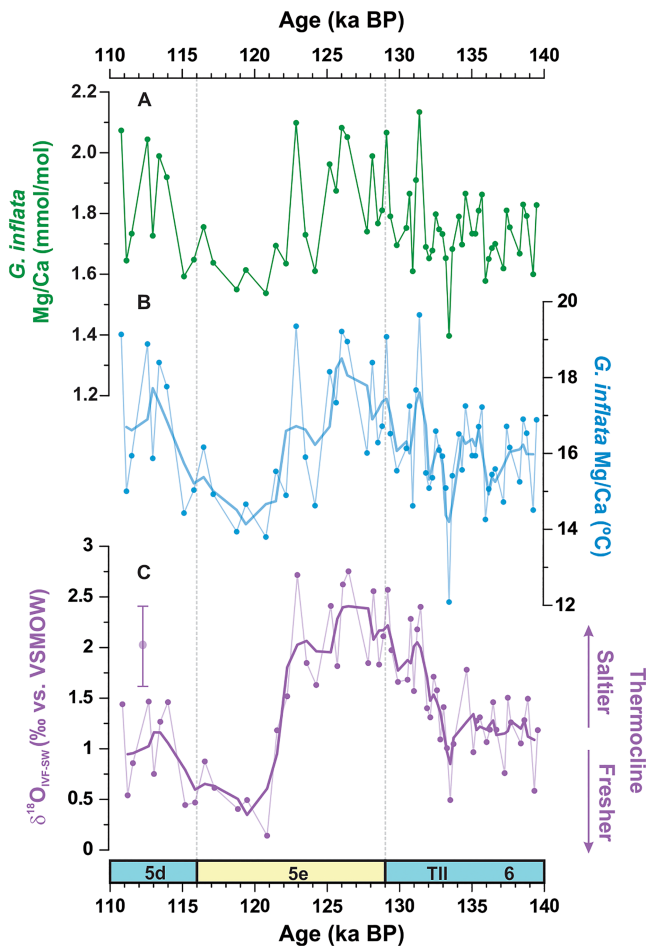
Figure 3. - Santos Basin thermocline conditions, as assessed from *Globorotalia inflata* shells in core GL-1090. A: *G. inflata* Mg/Ca ratio. B: Thermocline Mg/Ca ratio-derived temperatures. C: Ice-volume-corrected seawater $\delta^{18}O$ ($\delta^{18}O_{IVC-SW}$) values reconstructed from thermocline temperature (B) and the *G. inflata* $\delta^{18}O$ data published in Santos et al. (2017a). Mg/Ca ratio-derived temperature and $\delta^{18}O_{IVC-SW}$ 1σ uncertainties are indicated on the right- and left-hand sides of panels B and C, respectively. In panels B and C, the original records are depicted as dots connected by a thin line, and a three-point running average is presented as a thick line. The grey vertical dotted lines indicate the boundaries between Marine Isotope Stages (MIS) 6/5e and 5e/5d. MIS and Termination II (TII) are indicated at the bottom of the panel.

(Figure S3). This minor reduction in uncertainty at 1375 cm compared with that at 1404 cm is due to the impossibility of tying this portion of the core to a radiometric tie-point, as we did for the end of TII.

4. Results

The *G. inflata* Mg/Ca ratios ranged from 2.13 to 1.39 mmol/mol between 140 and 110 ka BP (Figure 3A). Values of approximately 1.7 mmol/mol occurred at the end of MIS 6, corresponding to a thermocline temperature of around 16 °C. From TII to early-MIS 5e, the *G. inflata* Mg/Ca ratio increased to approximately 2.0 mmol/mol, which corresponds to high temperature values of approximately 18 °C (Figure 3B). This high Mg/Ca ratio and corresponding temperature lasted until 126.4 ka BP, when they declined sharply to 1.6 mmol/mol and by 2 °C, respectively, until 124.2 ka BP. A brief interruption in the decreasing trend during this time period was shown by one sample, which presented a high Mg/Ca ratio (2.09 mmol/mol) at 122.9 ka BP, briefly restoring the thermocline to the warm values recorded during early-MIS 5e. Subsequently, *G. inflata* Mg/Ca ratios values decreased rapidly to approximately 1.6 mmol/mol. This second rapid decrease corresponds to a cooling of more than 2 °C in the thermocline, which remained at its coldest until the end of MIS 5e at 116 ka BP. In the transition to MIS 5d, the *G. inflata* Mg/Ca ratio increased once again to values around 2.0 mmol/mol (Figure 3A), corresponding to warm thermocline values of approximately 18 °C. This period of warming interrupted the cooling trend that prevailed below the surface waters of the Santos Basin throughout the end of the Last Interglacial period (Figure 3B).

Thermocline $\delta^{18}O_{IVC-SW}$ values fluctuated minimally around 1.0 ‰ between ca. 140 and 135 ka BP (Figure 3C). After ca. 135 ka BP, they increased from TII to early-MIS 5e, when they increased by approximately 1.5 ‰, reaching a maximal value of 2.75 ‰ at 126.4 ka BP. Similar to the decrease seen in the temperature record, we also observed a short-term decline in thermocline $\delta^{18}O_{IVC-SW}$ values between 126.4 and 124.2 ka BP. This reduced salinity was interrupted by a minor increase in $\delta^{18}O_{IVC-SW}$ values at 122.9 ka BP, which was subsequently followed by the least saline interval of the studied period that lasted until the end of MIS 5e. During this latter interval, thermocline $\delta^{18}O_{IVC-SW}$ values fluctuated around 0.5 ‰. Then, during MIS 5d, thermocline $\delta^{18}O_{IVC-SW}$ values increased to ~1.0 ‰ (Figure 3C), ending the prior trend of low salinity.

5. Discussion

5.1. Salinification of the Upper Subtropical South Atlantic Associated With Strengthening of the Agulhas Leakage

A 2D model of the AMOC (Weijer et al., 2001) showed that if the AL salt flux participates in the overturning, its salt content would leave the Atlantic by means of North Atlantic Deep Water (NADW) production. However, if the AL does not participate in the overturning, its salt would recirculate in the South Atlantic subtropical gyre and leave the Atlantic via the South Atlantic Current at approximately the same rate as it entered, so, comparatively, it would have a smaller influence on the overturning circulation (Weijer et al., 2001). To reconstruct propagation of AL signal across the South Atlantic subtropical gyre via its salt signature, we compared the surface (Santos et al., 2017b) and thermocline (this study) $\delta^{18}O_{IVC-SW}$ records of core GL-1090 with surface and thermocline records from core 64PE-174P13 of the Walvis Ridge (eastern South Atlantic) (Scussolini et al., 2015) (Figure 4).
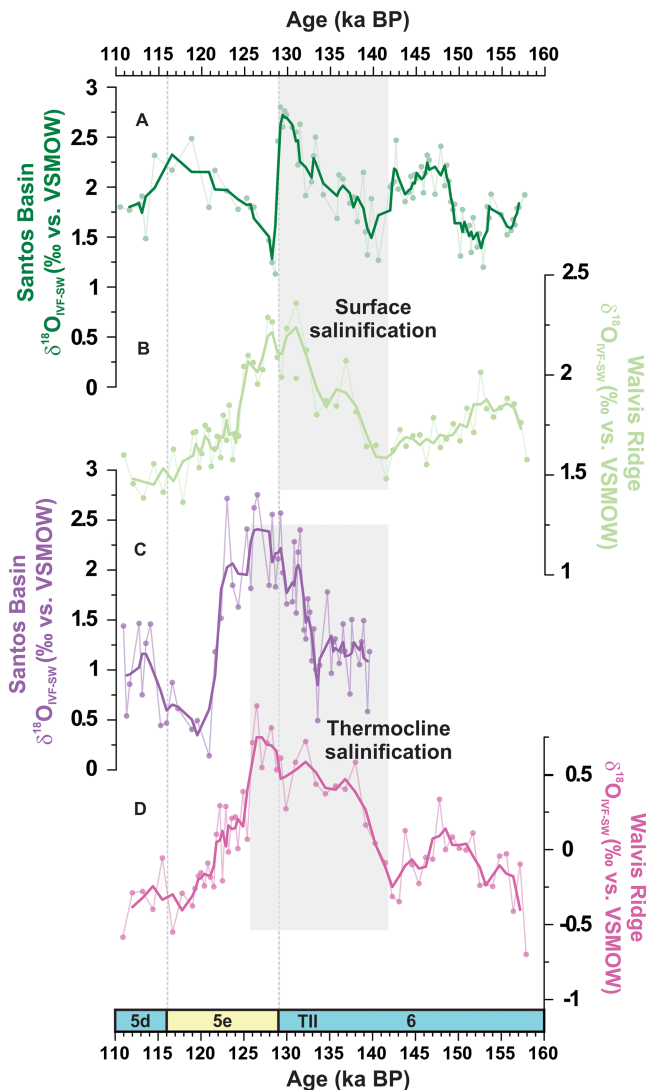
Figure 4. - Evolution of the surfaces and thermoclines of eastern (Walvis Ridge) and western (Santos Basin) South Atlantic ice-volume-corrected seawater $\delta^{18}O$ ($\delta^{18}O_{IVC-SW}$) values during the Marine Isotope Stage (MIS) 6/5e transition. A and B: Surface $\delta^{18}O_{IVC-SW}$ values from cores GL-1090 (A, Santos Basin) (Santos et al., 2017b) and 64PE-174P13 (B, Walvis Ridge) (Scussolini et al., 2015) estimated from Mg/Ca ratio-derived sea surface temperature and *Globigerinoides ruber* $\delta^{18}O$ values. C and D: Thermocline $\delta^{18}O_{IVC-SW}$ values from cores GL-1090 (C, Santos Basin) (this study) and 64PE-174P13 (D, Walvis Ridge) (Scussolini et al., 2015) estimated from thermocline Mg/Ca ratio-derived temperatures and *Globorotalia inflata* and *Globorotalia truncatulinoides* $\delta^{18}O$ values, respectively. Dots and thin lines represent the original data and a three-point running average is shown as a thick line. The grey vertical dashed lines indicate the boundaries between MIS 6/5e and 5e/5d. The grey bars highlight the intervals of surface and thermocline salinification in the eastern and western South Atlantic. MIS and Termination II (TII) are indicated at the bottom of the panel.

The rise in Walvis Ridge surface $\delta^{18}O_{IVC-SW}$ initiated at ca. 142 ka BP was mirrored by a near-simultaneous increase in Santos Basin surface $\delta^{18}O_{IVC-SW}$, and maximal values (i.e., saltiest conditions) at both locations occurred close to the end of TII (at 130–129 ka BP) (Figure 4A and B). During the period between 160–142 ka BP, when the AL was weaker (Scussolini et al., 2015), similarity of surface $\delta^{18}O_{IVC-SW}$ records between both sites is low, suggesting that the surface salinities of Santos Basin and Walvis Ridge evolved independently, so they were likely controlled by independent processes prior to 142 ka BP.

In the thermocline, our $\delta^{18}O_{IVC-SW}$ estimation suggests that from the end of MIS 6 to MIS 5e, highly saline waters were present below the surface in the western South Atlantic, similar to the conditions found in the eastern South Atlantic (Scussolini et al., 2015) (Figure 4C and D). Unfortunately, the period covered by our thermocline $\delta^{18}O_{IVC-SW}$ data is not sufficiently extensive to investigate possible similarities in the evolution of the salinities of the two basins prior to 142 ka BP. However, two features of the thermocline $\delta^{18}O_{IVC-SW}$ data from the GL-1090 and 64PE-174P13 cores suggest that they reflect basin-wide conditions. First, the peaks in thermocline salinity in both cores occurred later than those at the surface during early-MIS 5e (ca. 129 – 126 ka) (Figure 4C and D). This finding indicates that the influence of salty waters persisted longer in the thermocline than at the surface. Second, Scussolini et al. (2015) noted that the increase in $\delta^{18}O_{IVC-SW}$ at Walvis Ridge was ~70 % higher in the thermocline than at the surface, whereas we found it was ~80 % higher in Santos Basin. Together, these two findings suggest that massive salinification of the thermocline was a prominent feature across the subtropical South Atlantic during TII (Figure 4C and D).

The data from cores GL-1090 (Santos, et al., 2017b; this study) and 64PE-174P13 (Scussolini et al., 2015) (Figure 4) suggest a common forcing mechanism that increased the surface and thermocline salinities of both the eastern and western subtropical South Atlantic. These reconstructions reveal a geochemical fingerprint of the interaction between AL eddies and the BC. A recent census of Agulhas rings based on an algorithm for eddy detection evaluated the progression of several rings within a well-developed corridor in the South Atlantic between 23 and 35 °S (Guerra et al., 2018). That study examined the interaction between one of these rings and the BC using *in situ* measurements, and revealed that although saline anomalies may also be detected at the surface, the most substantial ones occurred at depths of 120–280 m and 360–600 m. This observation is consistent with the increase in surface salinity inferred from *G. ruber* data and the more substantial increase in thermocline salinity revealed by the *G. inflata* data. A high-resolution ocean model also supports these findings, since the contribution of the AL to the upper limb of the AMOC within the South Atlantic occurs mainly in central waters (Rühs et al., 2019). We propose that the increases in surface and thermocline salinity in the Santos Basin during TII and early-MIS 5e were a response to a more vigorous Indian Ocean-South Atlantic flow that likely increased the frequency of progressive rings from the AL into the western South Atlantic, as described by Guerra et al. (2018). The bulk of this inter-ocean exchange was concentrated in the thermocline, given that the most significant increase in $\delta^{18}O_{IVC-SW}$ values was attributed to the thermocline rather than at the surface.
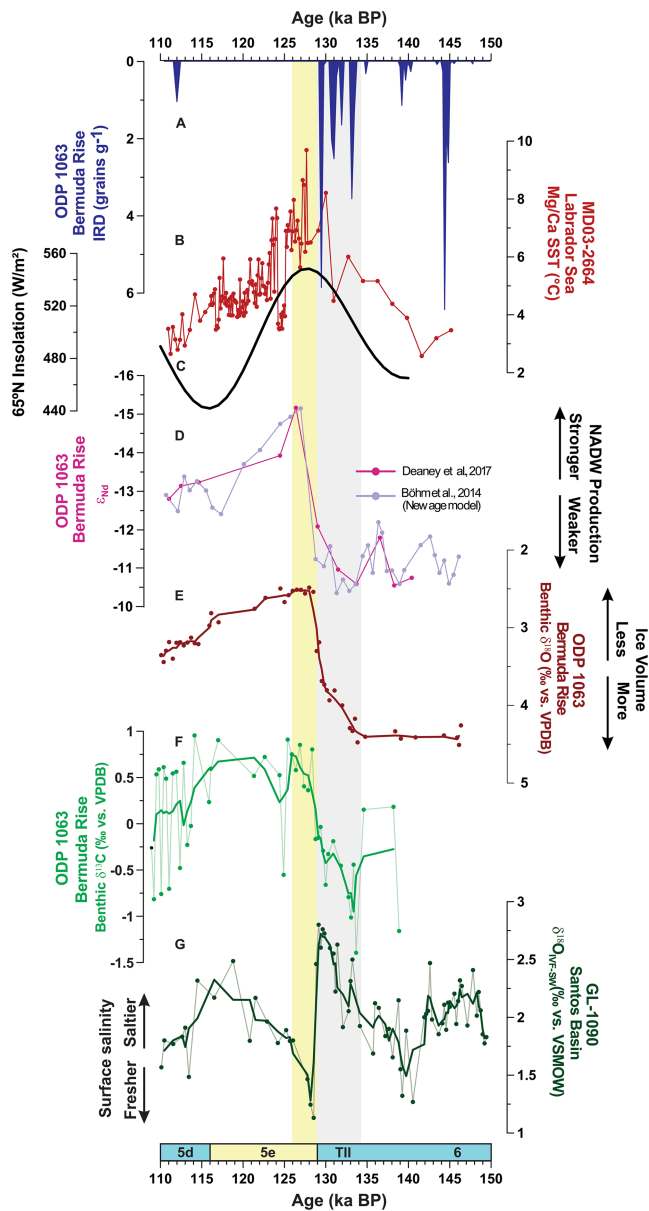
Figure 5. - Conditions associated with resumption of deep-water convection in the Labrador Sea during early-Marine Isotope Stage (MIS) 5e. A: Ice-rafted debris (IRD) from ODP Site 1063 (Deaney et al., 2017). B: Mg/Ca ratio-derived sea surface temperatures based on *Neogloboquadrina pachyderma* (sinistral) from core MD03-2664 (Irvalı et al., 2016). C: June 21 insolation at 65 °N (Berger, 1978). D: Neodymium isotopic composition (ε_{Nd}) from ODP Site 1063 [pink (Deaney et al., 2017) and purple (Böhm et al., 2015)]. E: *Cibicides wuellerstorfi* $\delta^{18}O$ data from ODP Site 1063 (Deaney et al., 2017). F: *C. wuellerstorfi* $\delta^{13}C$ data from ODP Site 1063 (Deaney et al., 2017). G: Surface $\delta^{18}O_{IVC-SW}$ values from core GL-1090 estimated from Mg/Ca ratio-derived sea surface temperatures and *Globigerinoides ruber* $\delta^{18}O$ values (Santos et al., 2017b). MIS and Termination II (TII) are indicated at the bottom of the panel. Dots and thin lines depict the original data and a three-point running average is shown by thick lines. The grey and yellow vertical bars highlight the periods of salt accumulation and salt release into the western South Atlantic, respectively.

Santos et al. (2017a) discussed patterns of the Santos Basin thermocline during the penultimate glacial-interglacial transition. They noted the presence of "glacial" $\delta^{18}O$ values in this region for a period of ca. 7 kyr after the onset of the Last Interglacial and formulated two possible reasons to explain that finding: (1) strong cooling of the thermocline due to the dynamics of the AMOC during this interval; or (2) discharge of salty waters sourced from the AL. Here, we confirm that it is this second explanation that accounts for the delayed glacial-interglacial transition.

5.2. Abrupt Bi-Phase Freshening of the Western South Atlantic and the AMOC During the Last Interglacial

Salt buildup in the western South Atlantic abruptly broke down during MIS 5e. Rapid reductions in $\delta^{18}O_{IVC-SW}$ at the surface at 129.1 ka BP and later in the thermocline after 122.9 ka BP illustrate robust freshening of the upper-waters of the Santos Basin (Figure 4A and C). Considering that the Last Interglacial was likely characterized by weaker monsoon precipitation over South America due to lower regional summer insolation (Cruz et al., 2005) and that the Santos Basin does not receive discharge from large rivers, it is unlikely that the surface water freshening was due to direct precipitation or continental freshwater input. Furthermore, ocean freshening due to either enhanced continental runoff or on-site precipitation cannot explain the subsequent decrease in $\delta^{18}O_{IVC-SW}$ values apparent in the thermocline. Thus, reorganization of the subtropical South Atlantic circulation is the most plausible explanation for the rapid decrease in upper ocean salinity of the western South Atlantic. That reorganization likely involved the re-circulatory route at the SEC bifurcation, which determines the volume of AL waters that flow south or north via the BC and NBC, respectively (Rühs et al., 2019). Flowing southwards with the BC, these salty waters could reach regions of the Subtropical Front, eventually being transferred into the Southern Ocean. However, an increase in upper ocean salinity in this region contradicts evidence indicating lower density water in the Southern Ocean during intervals of CO_2 release from the deep ocean around Antarctica (Adkins, 2013; Hayes et al., 2014). The most likely explanation for freshening of the upper ocean is increased export of salty waters into the Northern Atlantic. A regional recirculation cell within the subtropical gyre that drives northward transport in the upper 2000 m (Schmid, 2014) could have carried these salty waters, which accumulated over more than 10 kyr in the tropical Atlantic, until they reached the NBC before eventually leaving the South Atlantic.

Export of salty waters from the South Atlantic at the beginning of MIS 5e may have played a central role in oceanographic processes in high latitudes of the North Atlantic. Recent results from the Bermuda Rise (ODP Site 1063, subtropical North Atlantic) indicate the presence of very unradiogenic neodymium isotopic values at the beginning of MIS 5e, a significant decrease in benthic $\delta^{18}O$, and the occurrence of high benthic $\delta^{13}C$ in the deep ocean (4,584 m) (Böhm et al., 2015; Deaney et al., 2017) (Figure 5D-F). These data suggest that the return of deep-water convection (overshoot) in the Labrador Sea following interruption of melt-water discharge and ice-rafted debris of Heinrich Stadial (HS) 11 (Figure 5A) began ca. 128.7 ka BP and lasted less than 400 years. An Earth System model has indicated that under glacial boundary

conditions, this overshoot required transfer of salty waters from the tropical Atlantic (Gong et al., 2013), which potentially accumulated during the end of MIS 6 as a result of weakened overturning. These salty waters entered the southern Labrador Sea and induced hydrostatic instabilities that counterbalanced the influence of low-density meltwater (Govin, Braconnot, et al., 2012; Deaney et al., 2017). Features of the surface $\delta^{18}O_{IVC-SW}$ values from GL-1090 (Santos et al., 2017b) suggest that salty waters from the western South Atlantic may have contributed to propelling deep-ocean convection in the Labrador Sea upon development of favorable conditions (e.g., retraction of winter sea-ice cover). The similar timing of changes for cores GL-1090 and ODP Site 1063 supports this suggestion (Figure 5D-G). Santos Basin exhibited an abrupt decrease in surface salinity that developed over a short timeframe (129.1-128.5 ka BP) and occurred immediately after the end of the meltwater influx produced by HS 11 (Figure 5A and G). By updating the GL-1090 age model (Figure 2 and S3), we have generated an associated uncertainty of the same magnitude ($\pm$ 1.51 ka) as that determined for ODP Site 1063 ($\pm$ 1.72 ka) during the MIS 6/5e transition (Deaney et al., 2017). Caesar et al. (2018) showed that under current conditions, deep-ocean convection related to the AMOC is the main factor controlling evolution of surface temperatures in the subpolar North Atlantic. If this mechanism is robust through time and under different boundary conditions, then the peak values of surface temperatures in the Eirik Drift (core MD03-2664, southern Labrador Sea) (Irvalı et al., 2016) could also be interpreted as a signal of strong overturning (Figure 5B). An increase in surface $\delta^{18}O_{IVC-SW}$ values and peak warmth characterize the transition to the Last Interglacial, as indicated in many records from subpolar and subtropical North Atlantic waters (Oppo et al., 2006; Govin, Braconnot, et al., 2012; Mokeddem et al., 2014; Jiménez-Amat & Zahn, 2015). Despite these lines of evidence, it must also be recognized that there is no consensus on the existence of deep-ocean convection in the Labrador Sea, a topic that has been debated in other studies (Hillaire-Marcel et al., 2001; Rasmussen, 2003).

Although this episode of peak warmth and increased surface $\delta^{18}O_{IVC-SW}$ values may represent the return of deep-water formation in the Labrador Sea or only a transient event, it is essential to highlight that the high $\delta^{18}O_{IVC-SW}$ in surface waters flushed into the North Atlantic from the western South Atlantic probably originated from strenghtening of the AL. However, instead of being rapidly transported from the AL into the North Atlantic, these waters were stored temporarily (from ca. 142 ka BP) in the subtropical South Atlantic. Their subsequent release from the western South Atlantic eliminated the significant time difference between strengthening of the AL and the occurrence of deep-water formation (Deaney et al., 2017; Scussolini et al., 2015), with an immediacy such that marine records for the Indian Ocean-South Atlantic exchange and glacial-interglacial transitions are reconciled, at least for TII (Figure 5).

Despite the evidence for warm surface temperatures and an apparent AMOC overshoot in the Labrador Sea ca. 129 ka BP (Deaney et al., 2017; Irvalı et al., 2016), deep Atlantic circulation and peak interglacial conditions were later apparent in regions of the Nordic seas. Proxy and modeling studies have predicted a broad timeframe (ranging from 127 to 119 ka BP, i.e., mid- to late-MIS 5e) during which the Northeast Atlantic may have attained maximum interglacial conditions (Rasmussen et al., 2003; Bauch & Kandiano, 2007; Born et al., 2011; Govin, Braconnot, et al., 2012; Capron et al., 2014). As described above for the Labrador Sea, the Nordic seas also required salty Atlantic waters to resume and stabilize the formation of the highest density component of the NADW when the sea-ice retracted sufficiently to reduce freshwater inputs into high latitudes of the North Atlantic, thereby contributing to the establishment of favorable conditions for NADW production.

Bauch et al. (2000) proposed that transport of salty waters via the thermocline towards the Nordic seas was necessary, since the melting imposed by the Saalian ice-sheet during early-MIS 5e caused the surface ocean to become cold and stratified in this region, which forced subsurface water exchange between the subpolar Atlantic and Nordic seas. Our thermocline $\delta^{18}O_{IVC-SW}$ data from mid- to late-MIS 5e suggest the existence of another pulse of saline waters into the North Atlantic (but derived from the AL), which fits that scenario proposed by Bauch et al. (2000) (Figure 6D). This subsequent salt release started at 126.4 ka BP, but it was interrupted at 124.2 ka BP when the thermocline $\delta^{18}O_{IVC-SW}$ values returned to > 2.5 ‰. After 122.9 ka BP, salt release via the thermocline reached its maximum, resulting in a decrease of $\delta^{18}O_{IVC-SW}$ values by 2 ‰ to below 0.75 ‰ until ca. 115 ka BP (Figure 6F). This rapid decrease in salinity resulted in inputs of even denser waters into the North Atlantic compared to the earlier surface water freshening and may have helped to induce interglacial deep-water convection in the NE Atlantic.
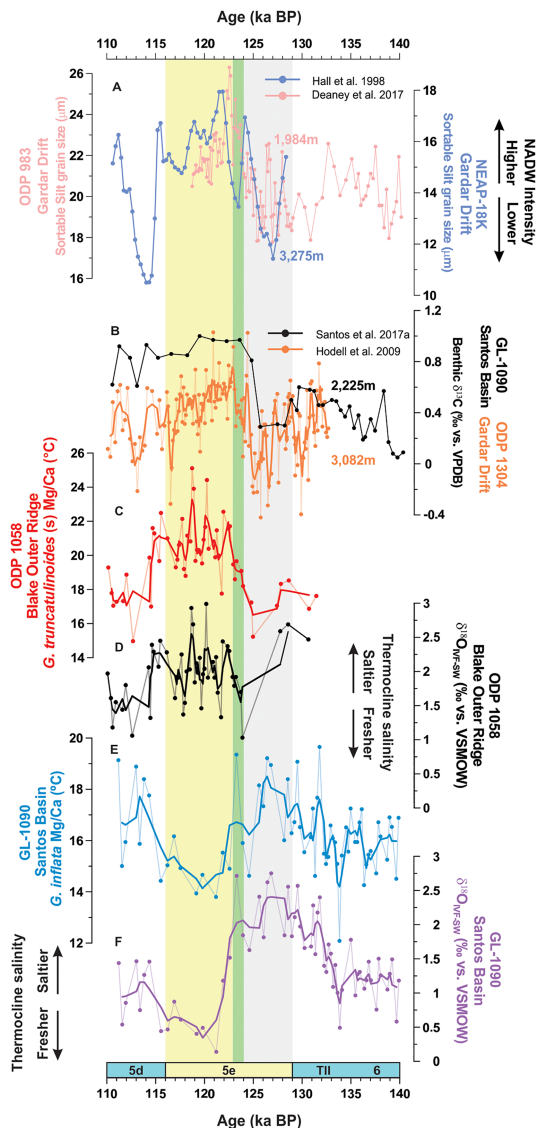
Figure 6. Thermocline ice-volume-corrected seawater $\delta^{18}O$ ($\delta^{18}O_{IVC-SW}$) values from the South Atlantic and resumption of the Atlantic Meridional Overturning Circulation (AMOC) during mid-Marine Isotope Stage (MIS) 5e. A: Sortable silt from core NEAP-18K (blue) (Hall et al., 1998) and ODP Site 983 (pink) (Deaney et al., 2017). B: *Cibicides wuellerstorfi* $\delta^{13}C$ values from GL-1090 (black) (Santos et al., 2017b) and ODP Site U1304 (orange) (Hodell et al., 2009). C: Thermocline Mg/Ca ratio-derived temperatures based on *Globorotalia truncatulinoides* data from ODP Site 1058 (Bahr et al., 2013). D: Thermocline ice-volume-corrected seawater $\delta^{18}O$ ($\delta^{18}O_{IVC-SW}$) values from ODP Site 1058 (Bahr et al., 2013). E: Thermocline Mg/Ca ratio-derived temperatures based on *Globorotalia inflata* data from core GL-1090 (this study). F: Thermocline ice-volume-corrected seawater $\delta^{18}O$ ($\delta^{18}O_{IVC-SW}$) values reconstructed from thermocline temperatures (E), taking into account the calcite *G. inflata* $\delta^{18}O$ data published in Santos et al. (2017a). MIS and Termination II (TII) are indicated at the bottom of the panel. Dots and thin lines depict the original data and three-point running averages are represented by thick lines. The grey and yellow vertical bars highlight the period of salt accumulation and salt release, respectively. The green bar highlights the millennial-scale event during which cooling and freshening of the western South Atlantic thermocline was briefly interrupted.

The freshening that occurred from ca. 123 ka BP was coeval to changes in deep-ocean circulation that are apparent in data on the speed of currents based on sortable silt records from ODP Site 983 and NEAP-18K and benthic $\delta^{13}C$ values from IODP Site U1304 (Deaney et al., 2017; Hall et al., 1998 ; Hodell et al., 2009) (all three of those datasets are from Gardar Drift in the Iceland Basin) (Figure 6A and B). The transition to a vigorous northern deep flux evidenced at NEAP-18K and IODP Site U1304 began ca. 125 ka BP (Hall et al., 1998; Hodell et al., 2009), with both these records showing a short millennial-scale interruption in this process ca. 124-123 ka BP (Figure 6A and B). This event was coeval to the high thermocline $\delta^{18}O_{IVC-SW}$ value in our data for Santos Basin between 124.2 and 122.9 ka BP (Figure 6A, B and F). Although the event is only evidenced by a single sample, the short interval might represent a brief slow-down in emptying of the western South Atlantic salt content in response to a rapid interruption in convection around the Nordic seas in mid-MIS 5e. Recent evidence from the East Greenland margin indicates persistent freshwater influx throughout MIS 5e (Zhuravleva et al., 2017). Higher-resolution reconstructions of the Last Interglacial in the western South Atlantic will be necessary to more thoroughly investigate this event. However, weakening of the AMOC mid-MIS 5e has not been detected in sortable silt of the ODP Site 983 record, instead shifting directly to its high values from ca. 124 ka BP (Deaney et al., 2017).

The absence or weakness of deep convection in the Nordic seas at the onset of MIS 5e would have also allowed stronger penetration of southern-sourced water into the deep Atlantic during the interval when our thermocline $\delta^{18}O_{IVC-SW}$ values were high. This observation corroborates benthic $\delta^{13}C$ data from GL-1090 (Santos et al., 2017b) and IODP Site U1304 (Hodell et al., 2009), which indicate that the deep Atlantic was still dominated by southern-sourced water below depths of ca. 2 km during early-MIS 5e (Figure 6B and F). Thus, the high $\delta^{13}C$ values of ODP Site 1063 (Deaney et al., 2017) (Figure 5F) demonstrate that the apparent overshoot of deep-water into the Labrador Sea at the beginning of MIS 5e neither filled eastern sites in the North Atlantic Basin nor had the necessary impetus to fill the mid-South Atlantic. Replacement of this ^{13}C-depleted signature in the deep Atlantic required a strong overturning, which may have been maintained after outflows from the western South Atlantic salt reservoir formed during TII and early-MIS 5e (Figure 6).

Discharge of salt toward the North Atlantic via thermocline waters, powered by the AL, is supported by the thermocline $\delta^{18}O_{IVC-SW}$ record from Blake Outer Ridge (ODP Site 1058, subtropical North Atlantic) that, unlike our data, indicates saltier conditions from mid- to late-MIS 5e (Bahr et al., 2013) (Figure 6D and F). The freshening estimated for the western South Atlantic thermocline from ca. 123 ka BP was also accompanied by a 4 °C cooling observed in the *G. inflata* Mg/Ca ratio-derived temperature, whereas thermocline temperatures increased at Blake Outer Ridge (Figure 6C and E). This 4 °C cooling is somewhat consistent with the millennial-scale South Atlantic response demonstrated in a transient model that simulated an abrupt resumption of the AMOC (Pedro et al., 2018), but it persisted for another couple of thousand years. Despite being accompanied by a consistent response in surface $\delta^{18}O_{IVC-SW}$ values, resumption of convection in the Labrador Sea was not accompanied by changes in surface temperature of the Santos Basin during

early-MIS 5e (Santos et al., 2017b). Instead, resumption of convection in Nordic seas occurred parallel to consistent changes of $\delta^{18}O_{IVC-SW}$ and temperature values of the western South Atlantic thermocline (Figure 6). This observation indicates that convection around the NE Atlantic more robustly modulates Atlantic salinity and temperature gradients. Direct measurements of the AMOC that were recently performed in the subpolar North Atlantic support this suggestion, revealing that the overturning across the subpolar NE Atlantic is approximately seven times greater than that across the subpolar NW Atlantic (Lozier et al., 2019). According to Crowley (1992), intensified production of the NADW during MIS 5e from 124 ka BP would have been accompanied by influx of warm waters from the Southern Hemisphere, with a polar amplification of the response in the South Atlantic. Hence, the interval between ca. 123 and 116 ka BP, i.e., when fresh and cold conditions dominated the western South Atlantic thermocline, coincided with a period of full deep-water convection in the North Atlantic (Figure 6). During that period, thermocline heat was likely transported northwards and released into the surface waters in regions of intense vertical mixing. Some of this heat may have contributed to sustaining a warm climate during the end of MIS 5e under decreasing Northern Hemisphere summer insolation (Born et al., 2011).

Assuming age uncertainties in core GL-1090 of ± 1.51 and ± 4.32 ka at 129.1 and 122.9 ka BP (Figure S2), respectively, and that all of the other records discussed here are susceptible to the same levels of uncertainty, it is difficult to confidently establish a causal relationship between upper-ocean freshening in the western South Atlantic and the return of deep-water formation in the North Atlantic. In terms of glacial-interglacial transitions, triggers from the Southern Hemisphere have been proposed as causing significant climate shifts (e.g., Knorr & Lohmann, 2003). In this context, the mass transport of the AL would have been important for transmitting low-latitude forcing toward an interglacial climate (Beck et al., 2018) into the North Atlantic, and the western boundary of the South Atlantic would have been the channel allowing such interhemispheric connectivity. Even if it occurred later than the resumption of deep-water convection, the salt transfer from the Indian Ocean over the period spanning TII and early MIS 5e could represent the primary difference between a strong AMOC during a traditional interstadial and those during full interglacial conditions. Therefore, the combination of new and published data presented here offers a solid framework for considering how the injection of salty AL waters into the Atlantic may represent a mechanism by which an interglacial mode for the AMOC could be sustained after a glacial termination (Figures 5 and 6).

5.3. The Role of Tropical Ocean-Atmosphere Coupling in Atlantic Inter-Hemispheric Salt and Heat Exchange

Considering the intensification of the AL since ca. 142 ka BP evidenced by our data, why was this salt anomaly recirculated in the BC instead of being immediately transmitted into the North Atlantic? To answer that question, we shift our attention to the system responsible for inter-hemispheric water exchange in the Atlantic, namely the bifurcation of the SEC on the eastern South American margin. The SEC bifurcation determines whether waters of the upper South Atlantic become part of the return flow of meridional overturning or if they recirculate within the South Atlantic subtropical gyre by favoring either the NBC or the BC, respectively (Marcello et al., 2018). A numerical simulation demonstrated that the latitude of the SEC bifurcation controls partitioning of SEC waters into the NBC or the BC and that shifting latitude primarily relates to variations in local wind stress curl associated with seasonal movements of the Intertropical Convergence Zone (ITCZ) (Rodrigues et al., 2007). During austral spring/summer, locally positive wind stress curl due to a more southerly ITCZ position generates an anomalous anticyclonic circulation pattern whose southward component near the western South Atlantic causes the SEC bifurcation to shift to lower latitudes (Rodrigues et al., 2007). This configuration reduces NBC transport in favor of the BC. A modeling comparison supports this possibility, predicting a stronger BC when the bifurcation is at its northernmost position of ca. 8 °S during the austral summer (Silva et al., 2009).

A pronounced southward displacement of the Atlantic ITCZ during HS, associated with a steep Atlantic meridional SST gradient and a dramatic reduction in NBC transport, are robust climatic responses to slowdown of the AMOC, as revealed by both modeling and paleoclimate reconstructions of HS 1 (Deplazes et al., 2013; Mulitza et al., 2017; Venancio et al., 2018; Zhang et al., 2011). A similar situation likely occurred during HS 11 when cold sea surface temperatures dominated high latitudes of the North Atlantic, shifting the ITCZ to a more southerly position. The East Asian monsoon was markedly reduced during HS 11 (Wang et al., 2008), whereas very wet conditions prevailed in NE Brazil (Wang et al., 2004). Therefore, we suggest that
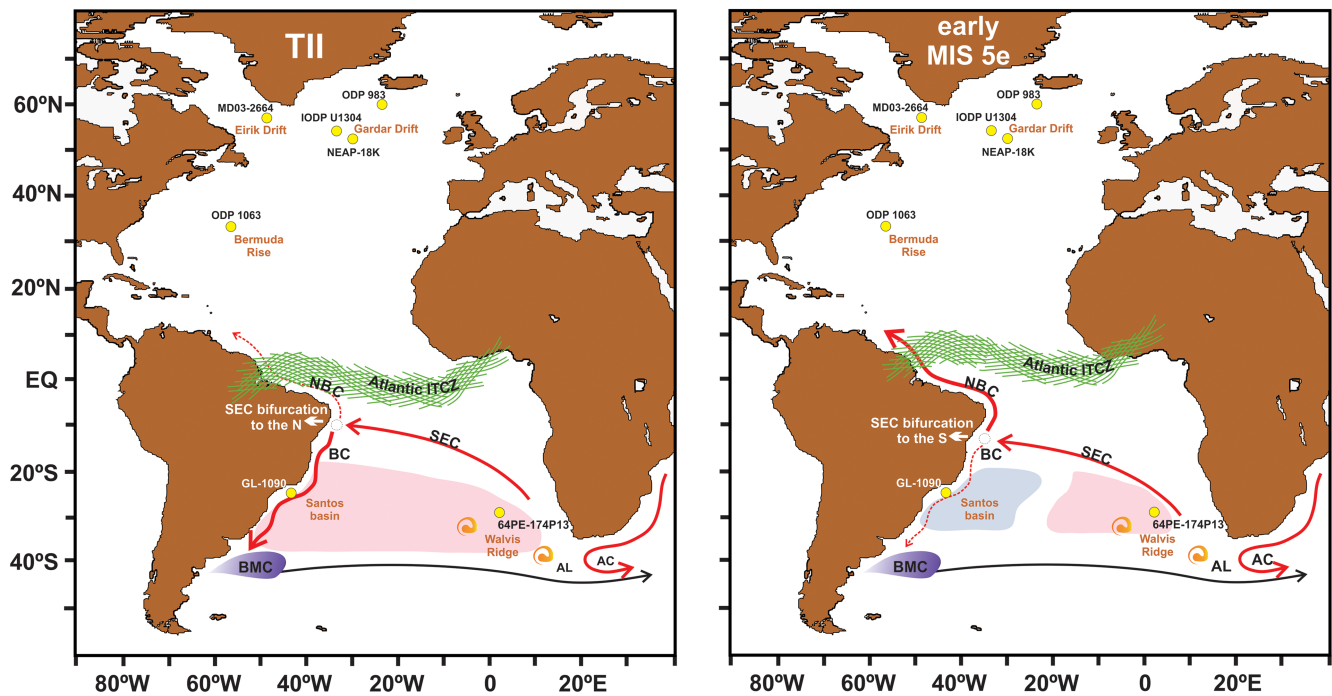
Figure 7. - Schematic of positions of the Intertropical Convergence Zone (ITCZ), surface circulation of the South Atlantic, and relative evolution of sea surface salinity during Termination II (left panel) and the early-Last Interglacial (right panel). The yellow dots show the positions of core GL-1090 (this study) and other cores discussed herein. Note that during Termination II (left panel), the more southerly ITCZ results in a northward shift of the South Equatorial Current (SEC) bifurcation, a stronger Brazil Current (BC), a weaker North Brazil Current (NBC), and storage of salty Agulhas Leakage (AL) waters within the South Atlantic subtropical gyre (area highlighted in red). At the onset of the Last Interglacial (right panel), the scenario changed rapidly so that the more northerly ITCZ led to a stronger NBC and weaker BC, thereby reducing salinity in the Santos Basin (highlighted in blue).

a southerly position of the ITCZ at the end of the penultimate glacial period produced austral spring/summer-like wind stress curl over the surface of the tropical South Atlantic, which shifted the SEC bifurcation to a more northerly position. This ocean-atmosphere coupling functioned as a "barrier" that enhanced flow of the BC and limited cross-equatorial transmission of the salty AL waters that recirculated within the South Atlantic subtropical gyre (Figure 7A). Redirection of salt anomalies into the BC also explains the similar evolution of surface and thermocline $\delta^{18}O_{IVC-SW}$ values between the western South Atlantic and the Walvis Ridge throughout TII (Figure 7A). Increased annual insolation at 65 °N from the end of MIS 6 to early-MIS 5e (Berger, 1978) likely attenuated temperature gradients between high and low latitudes. This change led to a reorganization of the tropical rain belt, including a northward shift of the ITCZ (Wang et al., 2008) and, consequently, southward movement of the SEC bifurcation (Figure 7B). These shifting positions strengthened the NBC, facilitating release of the salty waters stored in the surface subtropical gyre of the South Atlantic, which then contributed to the AMOC overshoot in the Labrador Sea at ca. 129 ka BP (Deaney et al., 2017) (Figure 7B).

The delayed release of salty thermocline waters by the western South Atlantic at ca. 123 ka BP involved processes that operated not only at the sea surface. Assuming that ITCZ movements are strongly tied to tropical insolation (Haug et al., 2001), shifting of the ITCZ to its northernmost position continued during the Last Interglacial when annual insolation reached its maximum at 10 °N (Berger, 1978). Today, the northern and southern hemisphere trade winds associated with Hadley circulation and ITCZ positioning play important roles in the dynamics and latitudinal limits of the North and South Atlantic subtropical cells (Green & Marshall, 2017). Furthermore, northward mass transport of the AMOC constantly drives the North Atlantic subtropical cell into higher latitudes, contributing to discharges of SACW into the tropical North Atlantic (Kirchner et al., 2009). Thus, the northernmost positioning of the ITCZ during the Last Interglacial would have facilitated northwards expansion of the South Atlantic subtropical cell, which likely favored freshening and cooling of the western South Atlantic thermocline. The reverse mechanism, i.e., southward

displacement of the North Atlantic subtropical cell, has been proposed to explain thermocline warming in the tropical North Atlantic during weakened overturning across the last deglaciation (Schmidt et al., 2012). Importantly, the SEC bifurcation dynamics we present in Figure 7 may also account for patterns of the South Atlantic subtropical cell, since nearly all equatorward thermocline flow passes through the western boundary as it is carried by NBC flux (Malanotte-Rizzoli et al., 2000).

6. Conclusion

Establishment of the Last Interglacial climate, which included a vigorous AMOC, occurred via two steps, with resumption of convection in the Labrador and Nordic seas during the early- and mid-MIS 5e, respectively. In conjunction with previously published data, our new records suggest that salty waters flushed into the Atlantic Ocean from the Indian Ocean during TII and early-MIS 5e can be detected in the western South Atlantic, where they were stored from the end of the penultimate glacial. Transmission of these dense saline waters into the North Atlantic probably accounted for dynamics of the AMOC during the Last Interglacial. Our study presents a framework in which strengthening of the AL can be linked to stabilization of the overturning that followed the penultimate glaciation. Furthermore, the cooling event recorded by our thermocline temperature reconstruction in mid- to late-MIS 5e indicates that the western South Atlantic subsurface was highly sensitive to recovery of the AMOC, as shown by model simulations. Identification of similar temperature declines in previous interglacials could provide insights into the timing of resumed deep convection (especially in the NE Atlantic) under different boundary conditions.

References

Adkins, J. F. (2013). The role of deep ocean circulation in setting glacial climates. *Paleoceanography*, *28*, 539–561. https://doi.org/10.1002/palo.20046

Anand, P., Elderfield, H., & Conte, M. H. (2003). Calibration of Mg/Ca thermometry in planktonic foraminifera from a sediment trap time series. *Paleoceanography*, *18*(2), 1050. https://doi.org/10.1029/2002PA000846

Bahr, A., Nürnberg, D., Karas, C., & Grützner, J. (2013). Millennial-scale versus long-term dynamics in the surface and subsurface of the western North Atlantic Subtropical Gyre during Marine Isotope Stage 5. *Global and Planetary Change*, *111*, 77–87. https://doi.org/10.1016/j.gloplacha.2013.08.013

Bard, E., & Rickaby, R. E. M. (2009). Migration of the subtropical front as a modulator of glacial climate. *Nature*, *460*(7253), 380–383. https://doi.org/10.1038/nature08189

Barker, S., Greaves, M., & Elderfield, H. (2003). A study of cleaning procedures used for foraminiferal Mg/Ca paleothermometry. *Geochemistry, Geophysics, Geosystems*, *4*(9), 8407. https://doi.org/10.1029/2003GC000559

Bauch, H. A., Erlenkeuser, H., Jung, S. J. A., & Thiede, J. (2000). Surface and deep water changes in the subpolar North Atlantic during Termination II and the Last Interglaciation. *Paleoceanography*, *15*(1), 76–84. https://doi.org/10.1029/1998PA000343

Bauch, H. A., & Kandiano, E. S. (2007). Evidence for early warming and cooling in North Atlantic surface waters during the last interglacial. *Paleoceanography*, *22*, PA1201. https://doi.org/10.1029/2005PA001252

Bazin, L., Landais, A., Lemieux-Dudon, B., Toyé Mahamadou Kele, H., Veres, D., Parrenin, F., et al. (2013). An optimized multi-proxy, multi-site Antarctic ice and gas orbital chronology (AICC2012): 120-800 ka. *Climate of the Past*, *9*(4), 1715–1731. https://doi.org/10.5194/cp-9-1715-2013

Beal, L. M., de Ruijter, W. P. M., Biastoch, A., & Zahn, R. (2011). On the role of the Agulhas system in ocean circulation and climate. *Nature*, *472*(7344), 429–436. https://doi.org/10.1038/nature09983

Beck, J., Zhou, W., Li, C., Wu, Z., White, L., Xian, F., et al. (2018). A 550,000-year record of East Asian monsoon rainfall from10Be in loess. *Science*, *360*(6391), 877–881. https://doi.org/10.1126/science.aam5825

Berger, A. (1978). Long-term variations of daily insolation and Quaternary climatic changes. *Journal of the Atmospheric Sciences*, *35*, 2362–2367. https://doi.org/10.1175/1520-0469(1978)035<2362:LTVODI>2.0.CO;2

Biastoch, A., Böning, C. W., & Lutjeharms, J. R. E. (2008). Agulhas leakage dynamics affects decadal variability in Atlantic overturning circulation. *Nature*, *456*(7221), 489–492. https://doi.org/10.1038/nature07426

Blaauw, M., & Christen, J. A. (2013). Bacon Manual - v2.2. Tutorial, 1–11.

Böhm, E., Lippold, J., Gutjahr, M., Frank, M., Blaser, P., Antz, B., et al. (2015). Strong and deep Atlantic meridional overturning circulation during the last glacial cycle. *Nature*, *517*(7532), 73–76. https://doi.org/10.1038/nature14059

Born, A., Nisancioglu, K. H., & Risebrobakken, B. (2011). Late Eemian warming in the Nordic Seas as seen in proxy data and climate models. *Paleoceanography*, *26*, PA2207. https://doi.org/10.1029/2010PA002027

Broecker, W. S., & Maier-Reimer, E. (1992). The influence of air and sea exchange on the carbon isotope distribution in the sea. *Global Biogeochemical Cycles*, *6*(3), 315–320. https://doi.org/10.1029/92GB01672

Byrne, D. A., Gordon, A. L., & Haxby, W. F. (1995). Agulhas eddies: A synoptic view using Geosat ERM data. *Journal of Physical Oceanography*, *25*, 902–917. https://doi.org/10.1175/1520-0485(1995)025<0902:AEASVU>2.0.CO;2

Caesar, L., Rahmstorf, S., Robinson, A., Feulner, G., & Saba, V. (2018). Observed fingerprint of a weakening Atlantic Ocean overturning circulation. *Nature*, *556*(7700), 191–196. https://doi.org/10.1038/s41586-018-0006-5

Caley, T., Giraudeau, J., Malaize, B., Rossignol, L., & Pierre, C. (2012). Agulhas leakage as a key process in the modes of Quaternary climate changes. *Proceedings of the National Academy of Sciences*, *109*(18), 6835–6839. https://doi.org/10.1073/pnas.1115545109

Caley, T., Peeters, F. J. C., Biastoch, A., Rossignol, L., van Sebille, E., Durgadoo, J., et al. (2014). Quantitative estimate of the paleo-Agulhas leakage. *Geophysical Research Letters*, *41*, 1238–1246. https://doi.org/10.1002/2014GL059278

Campos, B. E. J. D., Miller, J. L., Moiler, T. J., & Peterson, R. G. (1995). Physical oceanography of the Southwest Atlantic Ocean. *Current*, *8*(3), 87–91. https://doi.org/10.1063/1.3133352

Capron, E., Govin, A., Stone, E. J., Masson-Delmotte, V., Mulitza, S., Otto-Bliesner, B., et al. (2014). Temporal and spatial structure of multi-millennial temperature changes at high latitudes during the Last Interglacial. *Quaternary Science Reviews*, *103*, 116–133. https://doi.org/10.1016/j.quascirev.2014.08.018

Chiessi, C. M., Ulrich, S., Mulitza, S., Pätzold, J., & Wefer, G. (2007). Signature of the Brazil-Malvinas Confluence (Argentine Basin) in the isotopic composition of planktonic foraminifera from surface sediments. *Marine Micropaleontology*, *64*(1–2), 52–66. https://doi.org/10.1016/j.marmicro.2007.02.002

Cléroux, C., Cortijo, E., Anand, P., Labeyrie, L., Bassinot, F., Caillon, N., & Duplessy, J.-C. (2008). Mg/Ca and Sr/Ca ratios in planktonic foraminifera: Proxies for upper water column temperature reconstruction. *Paleoceanography*, *23*, PA3214. https://doi.org/10.1029/2007PA001505

Cléroux, C., Cortijo, E., Duplessy, J. C., & Zahn, R. (2007). Deep-dwelling foraminifera as thermocline temperature recorders. *Geochemistry, Geophysics, Geosystems*, *8*, Q04N11. https://doi.org/10.1029/2006GC001474

Cléroux, C., Demenocal, P., Arbuszewski, J., & Linsley, B. (2013). Reconstructing the upper water column thermal structure in the Atlantic Ocean. *Paleoceanography*, *28*, 503–516. https://doi.org/10.1002/palo.20050

Cortese, G., Abelmann, A., & Gersonde, R. (2007). The last five glacial-interglacial transitions: A high-resolution 450,000-year record from the subantarctic Atlantic. *Paleoceanography*, *22*, PA4203. https://doi.org/10.1029/2007PA001457

Crowley, T. J. (1992). North Atlantic Deep Water cools the southern hemisphere. *Paleoceanography*, *7*(4), 489–497. https://doi.org/10.1029/92PA01058

Cruz, F. W., Burns, S. J., Karmann, I., Sharp, W. D., Vuille, M., Cardoso, A. O., et al. (2005). Insolation-driven changes in atmospheric circulation over the past 116,000 years in subtropical Brazil. *Nature*, *434*(7029), 63–66. https://doi.org/10.1038/nature03365

Cunningham, S. A., Kanzow, T., Rayner, D., Baringer, M. O., Johns, W. E., Marotzke, J., et al. (2007). Temporal variability of the Atlantic Meridional Overturning Circulation at 26.5 N. *Science*, *317*(5840), 935–938. https://doi.org/10.1126/science.1141304

de Ruijter, W. P. M., Biastoch, A., Drijfhout, S. S., Lutjeharms, J. R. E., Matano, R. P., Pichevin, T., et al. (1999). Indian-Atlantic interocean exchange: Dynamics, estimation and impact. *Journal of Geophysical Research*, *104*(C9), 20,885–20,910. https://doi.org/10.1029/1998JC900099

Deaney, E. L., Barker, S., & van de Flierdt, T. (2017). Timing and nature of AMOC recovery across Termination 2 and magnitude of deglacial CO2 change. *Nature Communications*, *8*, 14595. https://doi.org/10.1038/ncomms14595

Deplazes, G., Lückge, A., Peterson, L. C., Timmermann, A., Hamann, Y., Hughen, K. A., et al. (2013). Links between tropical rainfall and North Atlantic climate during the last glacial period. *Nature Geoscience*, *6*(3), 213–217. https://doi.org/10.1038/ngeo1712

Donners, J., & Drijfhout, S. S. (2004). The Lagrangian view of South Atlantic interocean exchange in a global ocean model compared with inverse model results. *Journal of Physical Oceanography*, *34*(5), 1019–1035. https://doi.org/10.1175/1520-0485(2004)034<1019:TLVOSA>2.0.CO;2

Elderfield, H., & Ganssen, G. (2000). Past temperature and δ18O of surface ocean waters inferred from foraminiferal Mg/Ca ratios. *Nature*, *405*(6785), 442–445. https://doi.org/10.1038/35013033

Garzoli, S. L., & Matano, R. (2011). The South Atlantic and the Atlantic Meridional Overturning Circulation. *Deep Sea Research Part II: Topical Studies in Oceanography*, *58*(17–18), 1837–1847. https://doi.org/10.1016/j.dsr2.2010.10.063

Gebregiorgis, D., Hathorne, E. C., Sijinkumar, A. V., Nagender Nath, B., Nürnberg, D., & Frank, M. (2016). South Asian summer monsoon variability during the last ~54 kyrs inferred from surface water salinity and river run off proxies. *Quaternary Science Reviews*, *138*, 6–15. https://doi.org/10.1016/j.quascirev.2016.02.012

Gong, X., Knorr, G., Lohmann, G., & Zhang, X. (2013). Dependence of abrupt atlantic meridional ocean circulation changes on climate background states. *Geophysical Research Letters*, *40*, 3698–3704. https://doi.org/10.1002/grl.50701

Gordon, A. L. (1985). Indian-Atlantic transfer of thermocline water at the Agulhas Retroflection. *Science*, *227*(4690), 1030–1033. https://doi.org/10.1126/science.227.4690.1030

Govin, A., Braconnot, P., Capron, E., Cortijo, E., Duplessy, J. C., Jansen, E., et al. (2012). Persistent influence of ice sheet melting on high northern latitude climate during the early Last Interglacial. *Climate of the Past*, *8*(2), 483–507. https://doi.org/10.5194/cp-8-483-2012

Govin, A., Capron, E., Tzedakis, P. C., Verheyden, S., Ghaleb, B., Hillaire-Marcel, C., et al. (2015). Sequence of events from the onset to the demise of the Last Interglacial: Evaluating strengths and limitations of chronologies used in climatic archives. *Quaternary Science Reviews*, *129*, 1–36. https://doi.org/10.1016/j.quascirev.2015.09.018

Govin, A., Chiessi, C. M., Zabel, M., Sawakuchi, A. O., Heslop, D., Hörner, T., et al. (2014). Terrigenous input off northern South America driven by changes in Amazonian climate and the North Brazil Current retroflection during the last 250 ka. *Climate of the Past*, *10*(2), 843–862. https://doi.org/10.5194/cp-10-843-2014

Govin, A., Holzwarth, U., Heslop, D., Ford Keeling, L., Zabel, M., Mulitza, S., et al. (2012). Distribution of major elements in Atlantic surface sediments (36°N-49°S): Imprint of terrigenous input and continental weathering. *Geochemistry, Geophysics, Geosystems*, *13*, Q01013. https://doi.org/10.1029/2011GC003785

Grant, K. M., Rohling, E. J., Bar-Matthews, M., Ayalon, A., Medina-Elizalde, M., Ramsey, C. B., et al. (2012). Rapid coupling between ice volume and polar temperature over the past 150,000 years. *Nature*, *491*(7426), 744–747. https://doi.org/10.1038/nature11593

Greaves, M., Barker, S., Daunt, C., & Elderfield, H. (2005). Accuracy, standardization, and interlaboratory calibration standards for foraminiferal Mg/Ca thermometry. *Geochemistry, Geophysics, Geosystems*, *6*, Q02D13. https://doi.org/10.1029/2004GC000790

Green, B., & Marshall, J. (2017). Coupling of trade winds with ocean circulation damps ITCZ shifts. *Journal of Climate*, *30*(12), 4395–4411. https://doi.org/10.1175/JCLI-D-16-0818.1

Groeneveld, J., & Chiessi, C. M. (2011). Mg/Ca of Globorotalia inflata as a recorder of permanent thermocline temperatures in the South Atlantic. *Paleoceanography*, *26*, PA2203. https://doi.org/10.1029/2010PA001940

Groeneveld, J., Nürnberg, D., Tiedemann, R., Reichart, G.-J., Steph, S., Reuning, L., et al. (2008). Foraminiferal Mg/Ca increase in the Caribbean during the Pliocene: Western Atlantic Warm Pool formation, salinity influence, or diagenetic overprint? *Geochemistry, Geophysics, Geosystems*, *9*, Q01P23. https://doi.org/10.1029/2006GC001564

Guerra, L. A. A., Paiva, A. M., & Chassignet, E. P. (2018). On the translation of Agulhas rings to the western South Atlantic Ocean. *Deep Sea Research Part I: Oceanographic Research Papers*, *139*, 104–113. https://doi.org/10.1016/j.dsr.2018.08.005

Hall, I. R., McCave, I. N., Chapman, M. R., & Shackleton, N. J. (1998). Coherent deep flow variation in the Iceland and American basins during the last interglacial. *Earth and Planetary Science Letters*, *164*(1–2), 15–21. https://doi.org/10.1016/S0012-821X(98)00209-X

Haug, G. H., Hughen, K. A., Sigman, D. M., Peterson, L. C., & Röhl, U. (2001). Southward migration of the Intertropical Convergence Zone through the Holocene. *Science*, *293*(5533), 1304–1308. https://doi.org/10.1126/science.1059725

Hayes, C. T., Martínez-García, A., Hasenfratz, A. P., Jaccard, S. L., Hodell, D. A., Sigman, D. M., et al. (2014). A stagnation event in the deep South Atlantic during the last interglacial period. *Science*, *346*(6216), 1514–1517. https://doi.org/10.1126/science.1256620

Hillaire-Marcel, C., de Vernal, A., Bilodeau, G., & Weaver, A. J. (2001). Absence of deep-water formation in the Labrador Sea during the last interglacial period. *Nature*, *410*(6832), 1073–1077. https://doi.org/10.1038/35074059

Hodell, D. A., Minth, E. K., Curtis, J. H., McCave, I. N., Hall, I. R., Channell, J. E. T., & Xuan, C. (2009). Surface and deep-water hydrography on Gardar Drift (Iceland Basin) during the last interglacial period. *Earth and Planetary Science Letters*, *288*(1–2), 10–19. https://doi.org/10.1016/j.epsl.2009.08.040

Irvalı, N., Ninnemann, U. S., Kleiven, H. K. F., Galaasen, E. V., Morley, A., & Rosenthal, Y. (2016). Evidence for regional cooling, frontal advances, and East Greenland Ice Sheet changes during the demise of the last interglacial. *Quaternary Science Reviews*, *150*, 184–199. https://doi.org/10.1016/j.quascirev.2016.08.029

Jiménez-Amat, P., & Zahn, R. (2015). Offset timing of climate oscillations during the last two glacial-interglacial transitions connected with large-scale freshwater perturbation. *Paleoceanography*, *30*, 768–788. https://doi.org/10.1002/2014PA002710

Johns, W., Lee, T., & Beardsley, R. (1998). Annual cycle and variability of the North Brazil Current. *Journal of Physical Oceanography*, *28*, 103–128. https://doi.org/10.1175/1520-0485(1998)028%3C0103:ACAVOT%3E2.0.CO;2

Kirchner, K., Rhein, M., Hüttl-Kabus, S., & Böning, C. W. (2009). On the spreading of South Atlantic Water into the Northern Hemisphere. *Journal of Geophysical Research*, *114*, C05019. https://doi.org/10.1029/2008JC005165

Knorr, G., & Lohmann, G. (2003). Southern Ocean origin for the resumption of Atlantic thermohaline circulation during deglaciation. *Nature*, *424*(July), 532–536. https://doi.org/10.1038/nature01855

Kuhlbrodt, T., Griesel, A., Montoya, M., Levermann, A., Hofmann, M., & Rahmstorf, S. (2007). On the driving processes of the Atlantic meridional overturning circulation. *Reviews of Geophysics*, *45*, RG2001. https://doi.org/10.1029/2004RG000166

Kuhnert, H., Kuhlmann, H., Mohtadi, M., Meggers, H., Baumann, K., & Pätzold, J. (2014). Holocene tropical western Indian Ocean sea surface temperatures in covariation with climatic changes in the Indonesian region. *Paleoceanography*, *29*, 423–437. https://doi.org/10.1002/2013PA002555

Lea, D. W., Pak, D. K., & Paradis, G. (2005). Influence of volcanic shards on foraminiferal Mg/Ca in a core from the Galápagos region. *Geochemistry, Geophysics, Geosystems*, *6*, Q11P04. https://doi.org/10.1029/2005GC000970

Lisiecki, L. E., & Raymo, M. E. (2005). A Pliocene-Pleistocene stack of 57 globally distributed benthic δ18O records. *Paleoceanography*, *20*, PA1003. https://doi.org/10.1029/2004PA001071

Lončarić, N., Peeters, F. J. C., Kroon, D., & Brummer, G.-J. A. (2006). Oxygen isotope ecology of recent planktic foraminifera at the central Walvis Ridge (SE Atlantic). *Paleoceanography*, *21*, PA3009. https://doi.org/10.1029/2005PA001207

Lozier, M. S., Li, F., Bacon, S., Bahr, F., Bower, A. S., Cunningham, S. A., et al. (2019). A sea change in our view of overturning in the subpolar North Atlantic. *Science*, *363*(6426), 516–521. https://doi.org/10.1126/science.aau6592

Malanotte-Rizzoli, P., Hedstrom, K., Arango, H., & Haidvogel, D. B. (2000). Water mass pathways between the subtropical and tropical ocean in a climatological simulation of the North Atlantic ocean circulation. *Dynamics of Atmospheres and Oceans*, *32*(3–4), 331–371. https://doi.org/10.1016/S0377-0265(00)00051-8

Marcello, F., Wainer, I., & Rodrigues, R. R. (2018). South Atlantic Subtropical Gyre late twentieth century changes. *Journal of Geophysical Research: Oceans*, *123*, 5194–5209. https://doi.org/10.1029/2018JC013815

Martin, P. A., & Lea, D. W. (2002). A simple evaluation of cleaning procedures on fossil benthic foraminiferal Mg/Ca. *Geochemistry, Geophysics, Geosystems*, *3*(10), 8401. https://doi.org/10.1029/2001GC000280

McKenna, V. S., & Prell, W. L. (2004). Calibration of the Mg/Ca of Globorotalia truncatulinoides (R) for the reconstruction of marine temperature gradients. *Paleoceanography*, *19*, PA2006. https://doi.org/10.1029/2000PA000604

Mokeddem, Z., McManus, J. F., & Oppo, D. W. (2014). Oceanographic dynamics and the end of the last interglacial in the subpolar North Atlantic. *Proceedings of the National Academy of Sciences*, *111*(31), 11,263–11,268. https://doi.org/10.1073/pnas.1322103111

Mulitza, S., Chiessi, C. M., Schefuß, E., Lippold, J., Wichmann, D., Antz, B., et al. (2017). Synchronous and proportional deglacial changes in Atlantic meridional overturning and northeast Brazilian precipitation. *Paleoceanography*, *32*, 622–633. https://doi.org/10.1002/2017PA003084

Oppo, D. W., McManus, J. F., & Cullen, J. L. (2006). Evolution and demise of the Last Interglacial warmth in the subpolar North Atlantic. *Quaternary Science Reviews*, *25*(23–24), 3268–3277. https://doi.org/10.1016/j.quascirev.2006.07.006

Pedro, J. B., Jochum, M., Buizert, C., He, F., Barker, S., & Rasmussen, S. O. (2018). Beyond the bipolar seesaw: Toward a process understanding of interhemispheric coupling. *Quaternary Science Reviews*, *192*, 27–46. https://doi.org/10.1016/j.quascirev.2018.05.005

Peeters, F. J. C., Acheson, R., Brummer, G.-J. A., de Ruijter, W. P. M., Schneider, R. R., Ganssen, G. M., et al. (2004). Vigorous exchange between the Indian and Atlantic oceans at the end of the past five glacial periods. *Nature*, *430*(7000), 661–665. https://doi.org/10.1038/nature02785

Peterson, R. G., & Stramma, L. (1991). Upper-level circulation in the South Atlantic Ocean. *Progress in Oceanography*, *26*(1), 1–73. https://doi.org/10.1016/0079-6611(91)90006-8

Rasmussen, T. L. (2003). Deep sea records from the southeast Labrador Sea: Ocean circulation changes and ice-rafting events during the last 160,000 years. *Paleoceanography*, *18*(1), 1018. https://doi.org/10.1029/2001PA000736

Rasmussen, T. L., Thomsen, E., Kuijpers, A., & Wastegård, S. (2003). Late warming and early cooling of the sea surface in the Nordic seas during MIS 5e (Eemian Interglacial). *Quaternary Science Reviews*, *22*(8–9), 809–821. https://doi.org/10.1016/S0277-3791(02)00254-8

Regenberg, M., Steph, S., Nürnberg, D., Tiedemann, R., & Garbe-Schönberg, D. (2009). Calibrating Mg/Ca ratios of multiple planktonic foraminiferal species with δ18O-calcification temperatures: Paleothermometry for the upper water column. *Earth and Planetary Science Letters*, *278*(3–4324), –336. https://doi.org/10.1016/j.epsl.2008.12.019

Richardson, P. L. (2007). Agulhas leakage into the Atlantic estimated with subsurface floats and surface drifters. *Deep-Sea Research Part I: Oceanographic Research Papers*, *54*(8), 1361–1389. https://doi.org/10.1016/j.dsr.2007.04.010

Rodrigues, R. R., Rothstein, L. M., & Wimbush, M. (2007). Seasonal variability of the South Equatorial Current Bifurcation in the Atlantic Ocean: A numerical study. *Journal of Physical Oceanography*, *37*(1), 16–30. https://doi.org/10.1175/JPO2983.1

Rühs, S., Schwarzkopf, F. U., Speich, S., & Biastoch, A. (2019). Cold vs. warm water route — sources for the upper limb of the AMOC revisited in a high-resolution ocean model. *Ocean Science*, *15*, 489–512.

Santos, T. P., Lessa, D. O., Venancio, I. M., Chiessi, C. M., Mulitza, S., Kuhnert, H., & Albuquerque, A. L. S. (2017a). The impact of the AMOC resumption in the western South Atlantic thermocline at the onset of the Last Interglacial. *Geophysical Research Letters*, *44*, 547–554. https://doi.org/10.1002/2017GL074457

Santos, T. P., Lessa, D. O., Venancio, I. M., Chiessi, C. M., Mulitza, S., Kuhnert, H., et al. (2017b). Prolonged warming of the Brazil Current precedes deglaciations. *Earth and Planetary Science Letters*, *463*, 1–12. https://doi.org/10.1016/j.epsl.2017.01.014

Schmid, C. (2014). Mean vertical and horizontal structure of the subtropical circulation in the South Atlantic from three-dimensional observed velocity fields. *Deep-Sea Research Part I: Oceanographic Research Papers*, *91*, 50–71. https://doi.org/10.1016/j.dsr.2014.04.015

Schmidt, M. W., Chang, P., Hertzberg, J. E., Them, T. R., Ji, L., & Otto-Bliesner, B. L. (2012). Impact of abrupt deglacial climate change on tropical Atlantic subsurface temperatures. *Proceedings of the National Academy of Sciences*, *109*(36), 14,348–14,352. https://doi.org/10.1073/pnas.1207806109

Scussolini, P., Marino, G., Brummer, G.-J. A., & Peeters, F. J. C. (2015). Saline Indian Ocean waters invaded the South Atlantic thermocline during glacial termination II. *Geology*, *43*(2), 139–142. https://doi.org/10.1130/G36238.1

Shackleton, N. J. (1974). Attainment of isotopic equilibrium between ocean water and the benthonic foraminifera geuns Uvigerina: Isotopic changes in the ocean during the last glacial. Colloques Internationaux Du C.N.R.S., 219, 203–210.

Silva, M., Araujo, M., Servain, J., Penven, P., & Lentini, C. A. D. (2009). High-resolution regional ocean dynamics simulation in the southwestern tropical Atlantic. *Ocean Modelling*, *30*(4), 256–269. https://doi.org/10.1016/j.ocemod.2009.07.002

Steinke, S., Groeneveld, J., Johnstone, H., & Rendle-Bühring, R. (2010). East Asian summer monsoon weakening after 7.5 Ma: Evidence from combined planktonic foraminifera Mg/Ca and δ18O (ODP Site 1146; northern South China Sea). *Paleogeography, Palaeoclimatology, Palaeoecology*, *289*(1–4), 33–43. https://doi.org/10.1016/j.palaeo.2010.02.007

Stramma, L. (1991). Geostrophic transport of the South Equatorial Current in the Atlantic. *Journal of Marine Research*, *49*(2), 281–294. https://doi.org/10.1357/002224091784995864

Stramma, L., & England, M. (1999). On the water masses and mean circulation of the South Atlantic Ocean. *Journal of Geophysical Research*, *104*(C9), 20,863–20,883. https://doi.org/10.1029/1999JC900139

Stramma, L., Fischer, J., & Reppin, J. (1995). The north Brazil undercurrent. *Deep-Sea Research Part I: Oceanographic Research Papers*, *42*(5), 773–795. Retrieved from. http://www.sciencedirect.com/science/article/pii/096706379500014W

van Sebille, E., & van Leeuwen, P. J. (2007). Fast Northward Energy Transfer in the Atlantic due to Agulhas Rings. *Journal of Physical Oceanography*, *37*(9), 2305–2315. https://doi.org/10.1175/JPO3108.1

Vázquez Riveros, N., Govin, A., Waelbroeck, C., Mackensen, A., Michel, E., Moreira, S., et al. (2016). Mg/Ca thermometry in planktic foraminifera: Improving paleotemperature estimations for G. bulloides and N. pachyderma left. *Geochemistry, Geophysics, Geosystems*, *17*, 1249–1264. https://doi.org/10.1002/2015GC006234

Venancio, I. M., Belem, A. L., dos Santos, T. H. R., Zucchi, M. D. R., Azevedo, A. E. G., Capilla, R., & Albuquerque, A. L. S. (2014). Influence of continental shelf processes in the water mass balance and productivity from stable isotope data on the Southeastern Brazilian coast. *Journal of Marine Systems*, *139*(July), 241–247. https://doi.org/10.1016/j.jmarsys.2014.06.009

Venancio, I. M., Mulitza, S., Govin, A., Santos, T. P., Lessa, D. O., Albuquerque, A. L. S., et al. (2018). Millennial- to Orbital-Scale Responses of Western Equatorial Atlantic Thermocline Depth to Changes in the Trade Wind System Since the Last Interglacial. *Paleoceanography and Paleoclimatology*, *33*, 1490–1507. https://doi.org/10.1029/2018PA003437

Veres, D., Bazin, L., Landais, A., Toyé Mahamadou Kele, H., Lemieux-Dudon, B., Parrenin, F., et al. (2013). The Antarctic ice core chronology (AICC2012): an optimized multi-parameter and multi-site dating approach for the last 120 thousand years. *Climate of the Past*, *9*(4), 1733–1748. https://doi.org/10.5194/cp-9-1733-2013

Wang, X., Auler, A. S., Edwards, R. L., Cheng, H., Cristalli, P. S., Smart, P. L., et al. (2004). Wet periods in northeastern Brazil over the past 210 kyr linked to distant climate anomalies. *Nature*, *432*(7018), 740–743. https://doi.org/10.1038/nature03067

Wang, Y., Cheng, H., Edwards, R. L., Kong, X., Shao, X., Chen, S., et al. (2008). Millennial- and orbital-scale changes in the East Asian monsoon over the past 224,000 years. *Nature*, *451*(7182), 1090–1093. https://doi.org/10.1038/nature06692

Weijer, W. (2002). Response of the Atlantic overturning circulation to South Atlantic sources of buoyancy. *Global and Planetary Change*, *34*(3–4), 293–311. https://doi.org/10.1016/S0921-8181(02)00121-2

Weijer, W., De Ruijter, W. P. M., & Dijkstra, H. A. (2001). Stability of the Atlantic Overturning Circulation: Competition between Bering Strait freshwater flux and Agulhas heat and salt sources. *Journal of Physical Oceanography*, *31*(8), 2385–2402. https://doi.org/10.1175/1520-0485(2001)031<2385:SOTAOC>2.0.CO;2

Weijer, W., De Ruijter, W. P. M., Sterl, A., & Drijfhout, S. S. (2002). Response of the Atlantic overturning circulation to South Atlantic sources of buoyancy. *Global and Planetary Change*, *34*(3–4), 293–311. https://doi.org/10.1016/S0921-8181(02)00121-2

Weldeab, S., Schneider, R. R., & Kölling, M. (2006). Comparison of foraminiferal cleaning procedures for Mg/Ca paleothermometry on core material deposited under varying terrigenous-input and bottom water conditions. *Geochemistry, Geophysics, Geosystems*, 7, Q04P12. https://doi.org/10.1029/2005GC000990

Zhang, D., Msadek, R., McPhaden, M. J., & Delworth, T. (2011). Multidecadal variability of the North Brazil Current and its connection to the Atlantic meridional overturning circulation. *Journal of Geophysical Research*, *116*, C04012. https://doi.org/10.1029/2010JC006812

Zhuravleva, A., Bauch, H. A., & Van Nieuwenhove, N. (2017). Last Interglacial (MIS5e) hydrographic shifts linked to meltwater discharges from the East Greenland margin. *Quaternary Science Reviews*, *164*, 95–109. https://doi.org/10.1016/j.quascirev.2017.03.026